Voltage dependence of the Chara proton pump revealed by current-voltage measurement during rapid metabolic blockade with cyanide. J Membr Biol 114:205-223

ARTICLE *in* JOURNAL OF MEMBRANE BIOLOGY · MAY 1990

Impact Factor: 2.46 · Source: PubMed

3 AUTHORS, INCLUDING:

Mary Jane Beilby
University of New South Wales
72 PUBLICATIONS **1,451** CITATIONS
SEE PROFILE

Mark Tester
King Abdullah University of Science and Te…
169 PUBLICATIONS **12,191** CITATIONS
SEE PROFILE

J. Membrane Biol. 114, 205–223 (1990)

The Journal of
Membrane Biology

Voltage Dependence of the *Chara* Proton Pump Revealed by Current-Voltage Measurement During Rapid Metabolic Blockade with Cyanide

Michael R. Blatt,* Mary J. Beilby,** and Mark Tester
Botany School, University of Cambridge, Cambridge CB2 3EA, England

Summary. It is generally agreed that solute transport across the *Chara* plasma membrane is energized by a proton electrochemical gradient maintained by an H^+-extruding ATPase. Nonetheless, as deduced from steady-state current-voltage (*I-V*) measurements, the kinetic and thermodynamic constraints on H^+-ATPase function remain in dispute. Uncertainties necessarily surround long-term effects of the relatively nonspecific antagonists used in the past; but a second, and potentially more serious problem has sprung from the custom of subtracting, across the voltage spectrum, currents recorded following pump inhibition from currents measured in the control. This practice must fail to yield the true *I-V* profile for the pump when treatments alter the thermodynamic pressure on transport.

We have reviewed these issues, using rapid metabolic blockade with cyanide and fitting the resultant whole-cell *I-V* and difference-current-voltage (*dI-V*) relations to a reaction kinetic model for the pump and parallel, ensemble leak. Measurements were carried out after blocking excitation with $LaCl_3$, so that steady-state currents could be recorded under voltage clamp between −400 and +100 mV. Exposures to 1 mM NaCN (CN) and 0.4 mM salicylhydroxamic acid (SHAM) depolarized (positive-going) *Chara* membrane potentials by 44–112 mV with a mean half time of 5.4 ± 0.8 sec (n = 13). ATP contents, which were followed in parallel experiments, decayed coincidently with a mean half time of 5.3 ± 0.9 sec ($[ATP]_{t=0}$, 0.74 ± 0.3 mM; $[ATP]_{t=\infty}$, 0.23 ± 0.02 mM). Current-voltage response to metabolic blockade was described quantitatively in context of these changes in ATP content and the consequent reduction in pump turnover rate accompanied by variable declines in ensemble leak conductance. Analyses of *dI-V* curves (±CN+SHAM) as well as of families of *I-V* curves taken at times during CN+SHAM exposures indicated a stoichiometry for the pump of one charge (H^+) transported per ATP hydrolyzed and an equilibrium potential near −420 mV at neutral external pH; under these conditions, the pump accounted for approximately 60–75% of the total membrane conductance near V_m. Complementary results were obtained also in fitting previously published *I-V* data gathered over the external pH range 4.5–7.5. Kinetic features deduced for the pump were dominated by a slow step preceding H^+ unloading outside, and by recycling and loading steps on the inside which were in rapid equilibrium. These characteristics predict, in marked contrast to the situation for *Neurospora*, that cytoplasmic acid loads in *Chara* should shift the pump *I-V* curve negative-going along the voltage axis with little change in maximum current output at positive voltages.

Key Words *Chara* · reaction kinetic carrier model · H^+-ATPase · (difference) current-voltage analysis · nonlinear leak · ATP · intracellular pH · extracellular pH

Introduction

Transport at the plasma membrane of higher plant cells, of many algae and of fungi is held to be energized by the proton electrochemical gradient and maintained by ATP hydrolysis coupled to a vectorial flux of H^+ out of the cells. Proton-extruding ATPases now have been isolated and cloned from the plasma membranes of yeast (Serrano, Kielland-Brandt & Fink, 1986) and *Neurospora* (Hager et al., 1986); these H^+ pumps are "E_1-E_2" class enzymes, like the Na^+/K^+-ATPase and Ca^{2+}-ATPase of animal tissues, and are characterized by a quasi-stable, phosphorylated intermediate.

For the moment, there are only indirect indications for a H^+-ATPase at the plasma membrane of *Chara*, but the circumstantial evidence is overwhelming. Near neutral external pH, stable membrane potentials recorded with intracellular microelectrodes frequently lie well negative to all dominant diffusion potentials and are sensitive to metabolic inhibition and to pH (*cf.* Spanswick, 1972, 1974; Richards & Hope, 1974); Characean algae acidify stagnant media (Spear, Barr & Barr, 1969); furthermore, ATP is necessary to maintaining the large, negative membrane potential and the proton current (Shimmen & Tazawa, 1977, 1980;

* *Current address:* Department of Biochemistry and Biological Sciences, Wye College, University of London, Wye (Ashford), Kent TN25 5AH, England.

** *Current address:* School of Biological Sciences, University of Sydney, Sydney N.S.W. 2006, Australia.

Kawamura, Shimmen & Tazawa, 1980; Takeshige, Shimmen & Tazawa, 1986).

It would seem reasonable to conclude that the *Chara* H^+ pump, like that of *Neurospora* (*cf.* Slayman & Sanders, 1985), transports one H^+ out of the cell per ATP hydrolyzed. Membrane potentials have been reported in excess of (−)350 mV (Lucas, 1982), a figure thermodynamically improbable for a pump with a stoichiometry of $2(H^+):1(ATP)$ but well within the approximate (−)500-mV ceiling estimated for a $1(H^+):1(ATP)$ pump.

No consensus has been reached, however, about the contribution the pump makes to the total membrane conductance (for discussions, *see* Spanswick, 1981; Beilby, 1984). At least some of the discord probably arises because the pump conductance itself is voltage dependent. Beilby (1984) suggested that the pump made up about half of the total membrane (slope) conductance near the free-running (resting) potential when pH_o was close to neutrality. Her measurements were obtained under voltage (and space) clamp after rendering the cells inexcitable so that steady-state current-voltage (*I-V*) data could be gathered over an extended voltage range (nearly 500 mV!). The results clearly showed in the whole-membrane (slope) conductance-voltage (*G-V*) profile a broad maximum near −200 mV which was shifted, positive-going with acid pH_o and which could be eliminated with diethylstilbesterol (DES).

Kishimoto et al. (1984) and Takeuchi et al. (1985) used a similar approach, although the *I-V* scans were limited to a very narrow voltage range and, in this case, dicyclohexylcarbodiimide (DCCD) was used to isolate pump current. Yet, they concluded that the vast bulk of total membrane conductance was attributable to the pump. The discord is still more striking because, in their kinetic analyses of pump *I-V* relations, Kishimoto et al. (1984) arrived at a stoichiometry of $2(H^+):1(ATP)$ while Beilby (1984) concluded that her data were consistent with a $1(H^+):1(ATP)$ pump.

One difficulty confronted generally in assessing H^+-pump activities in plants and fungi is the lack of any selective inhibitor. The problem is further compounded, in these *Chara* studies, by the long exposures to the drugs used to "block" the pump. Dicyclohexylcarbodiimide blocks mitochondrial and chloroplast ATPases as well as the H^+-ATPase of the plasma membrane (*cf.* Sze, 1985). In turn, DES is known to affect current passage through *Chara* "K^+-state" K^+ channels (Beilby, 1986) and background (K^+) conductance (Beilby, 1984; Bisson, 1986); DES also progressively blocks K^+ channel current in stomatal guard cells (Blatt, 1988*b*). Clearly, any changes in these "leak" currents would have distorted the apparent pump *I-V* characteristics, since the measure of H^+ pump current in both studies depended on subtracting leak currents recorded in the presence of the inhibitors from the whole-cell *I-V* relations measured prior to the treatments. Changes in leak conductance are an obvious explanation for the high stoichiometries Kishimoto et al. (1984) obtained with DCCD.

There is, in addition, a more subtle complication to these analyses which raises a fundamental question about their validity; in both cases, it was assumed that little or no current flowed through the pump *at any voltage* following treatments with the inhibitors. In fact, Beilby (1984) found that subtracting currents often revealed, for the pump, *I-V* (or more precisely, difference-current-voltage) relations which failed to cross the voltage axis and even showed increasingly positive (outward) currents at voltages approaching −400 mV. Precisely this behavior is expected of difference *I-V* (*dI-V*) profiles when experimental manipulations alter the electrochemical driving force for transport (Chapman, Johnson & Kootsey, 1983; Blatt, 1986). Under these conditions, current is not affected uniformly across the voltage spectrum and *no* indication of the transporter equilibrium (or zero-current) potential (in this case, E_p), and hence of transport stoichiometry, can be expected in the *dI-V* curve itself.

In the present study, we sought to review these issues and to identify the dominant voltage-dependent kinetic features of the *Chara* H^+ pump, using rapid metabolic blockade with cyanide (CN) to dissect the whole-cell *I-V* relations into their component pump and leak currents. Our choice of CN was founded not on a basis of selectivity, but rather on the assumption that a fall in the cellular ATP pool should be detected first in charge movements coupled directly to the hydrolysis of ATP. In fact, measurements carried out before, and over the course of exposures to CN yielded *I-V* and *dI-V* (±CN) profiles which were at least qualitatively comparable to the data gathered previously with DES (Beilby, 1984).

Quantitatively, however, fitting the *I-V* and *dI-V* curves to an explicit reaction kinetic carrier model for the pump gave quite different results, when analyzed both by least-squares minimization and by a semi-analytical approach. The outcome, in both cases, was consistent with a transport cycle in which transit between carrier states was dominated neither by membrane charge transfer reactions nor by the voltage-insensitive limb of the reaction cycle. The same conclusion was drawn also from analyses of some previously published *I-V* curves (Beilby, 1984). [Data gathered over a relatively narrow voltage range (Kishimoto et al., 1984; Takeuchi et al.,

1985) precluded an unambiguous assessment of the kinetic and thermodynamic properties for the pump (*see* Hansen et al., 1981; Blatt, 1986).] These results bring the *Chara* pump in line with characteristics deduced for primary charge transport in *Vicia* stomatal guard cells (Blatt, 1987) and highlight some kinetic differences from the H^+ pump of *Neurospora* (*cf.* Gradmann, Hansen & Slayman, 1982; Slayman & Sanders, 1985). The data also support a stoichiometry of 1(H^+): 1(ATP) for the pump.

Materials and Methods

Cell Culture and Experimental Protocol

Chara corallina was grown in standard APW (0.1 mM KCl, 1.0 mM NaCl, 0.5 mM $CaCl_2$) on the roof of the Botany School. Young leaf cells were used for experimentation. These were kept in APW for approximately 24 hr prior to the start of the experiment.

All measurements were carried out in rapidly flowing solutions (10 ml/min ≅ 30 chamber vol/min) against a background light intensity of 100 μmol m^{-2} sec^{-1} (light from a fiber optic light source. Intralux 150 Volpi, calculated as the middle of the visible spectrum) at the ambient temperature, 20–22°C. Experimental solutions were buffered with 5 mM 2-(N-morpholino)propanesulfonic acid (MES) adjusted to pH 5.5 with NaOH (5 mM Na-MES). Cyanide was added as the sodium salt to a final concentration of 1.0 mM immediately before experiments and the pH was readjusted as necessary. Salicylhydroxamic acid (SHAM, 0.4 mM) was included to block alternate oxidase pathways for electron transport. SHAM was prepared as a 0.4-M stock solution in ethanol, and was diluted 1000-fold for use. Controls with 0.1% (vol/vol) ethanol showed no measureable effect of the solvent when added alone. Surface areas were calculated from the orthogonal dimensions (diameter, length) of impaled cells measured with a calibrated eyepiece micrometer.

Following impalements with the current-passing and voltage-recording electrodes, the cells were exposed to 0.05–0.1 mM $LaCl_3$ for periods of 20–40 min to block excitation (Beilby, 1984). Once the cells were rendered inexcitable, they were returned to the standard APW and the membrane characteristics were monitored until stable (1–2 hr). In general, $LaCl_3$ treatments had no lasting effect on the resting membrane characteristics but, by blocking excitation, it became possible to extend current-voltage scans to potentials well positive of 0 mV (Beilby, 1984).

ATP

The ATP contents of single *Chara* leaf cells were determined by luciferin-luciferase assay, in a modification of the method described by Scott and Ellar (1978). The cells were prepared as above and transferred, one at a time, to a rapidly flowing solution of APW buffered with 5 mM Na-MES, pH 5.5, or to the same medium with 0.4 mM SHAM ± 1 mM NaCN. At various times thereafter each treatment was terminated by removing the cell and placing it in a test tube containing 2 ml of boiling propan-2-ol (85°C). Cells were extracted at this temperature for 5 min and then frozen in liquid nitrogen and freeze-dried at −60°C.

Luciferin-luciferase assays were carried out with Tris-aspartate buffered reagents (Sigma, St. Louis, MO). Cell extracts were rehydrated in 0.5 ml of 50 mM Tris-aspartate, pH 7.75, and vortexed. Cell walls were removed with tweezers. ATP-dependent luminescence was followed over time with an LKB Wallac 1250 Luminometer (LKB, Stockholm) and strip chart recorder. The magnitude of the luminescence peak, which occurred 2–3 sec after adding the reagents, was used to quantify the signal. Calibrations were carried out with equivalent buffer volumes containing 0.1–10 pmol ATP. Over this range the signal was linear with ATP content. Aliquots from the cell extractions were diluted appropriately to fall within this range. Internal and separate standards, added at extraction times, indicated yields for ATP of 92 ± 3% (n = 5).

Electrical

The apparatus and mechanical operations have been described in detail (Beilby & Beilby, 1983; Beilby, 1984). The clamp circuit accepted commands from a MINC 11 computer, which also logged both the membrane potential and the clamp current. Current-voltage (*I-V*) measurements were carried out by space-clamping cells to a bipolar staircase of pulses while sampling trans-plasma-membrane voltage and current every 2 msec. Pulses of 60-msec duration were sufficient for the clamp current to reach quasi-steady state in APW (Beilby, 1984, 1990). For technical reasons, arming the command voltage staircase required an initial, stable potential reading. So, *I-V* scans could be run only after some 60 sec into CN+SHAM treatments. The limitation did not complicate the analyses, however, for reasons detailed in Results.

Numerical Analysis

Current-voltage relations were fitted to 8th-order polynomials by nonlinear, least-squares (Marquardt, 1963; Jennings et al., 1988). Difference-current-voltage (*dI-V*) curves for the pump were derived by subtracting fitted *I-V* data as indicated in Results. Slope conductance-voltage (*G-V*) characteristics were obtained by differentiating the fitted *I-V* or *dI-V* curves.

Current-voltage characteristics for the pump were extracted by fitting the data to an explicit reaction-kinetic carrier model for the pump and parallel leak (taken to represent the sum of all other current pathways in the membrane, whether of channels or coupled secondary transporters). Two separate approaches were used. In the first approach, pump *dI-V* curves (±CN+SHAM) were fitted using a semi-analytical method and the parameter estimates were subsequently translated to the experimental *I-V* data assuming a linear leak profile (Blatt, 1987). In the second, families of whole-cell *I-V* curves, gathered before and during exposures to CN+SHAM, were fitted using a modified Simplex algorithm (Nelder & Mead, 1965; Press et al., 1986). This algorithm is highly opportunistic, but proved robust so long as the initial parameter estimates were nondegenerate, i.e., were spread over a sufficiently wide range of values (*see* Press et al., 1986). As a check against early convergence or local minima, fittings were restarted at least three and occasionally 4–6 times—with secondary estimates chosen randomly within a range 10^1- to 10^3-fold above and below the previously fitted value—until trials converged on a common set of parameters.

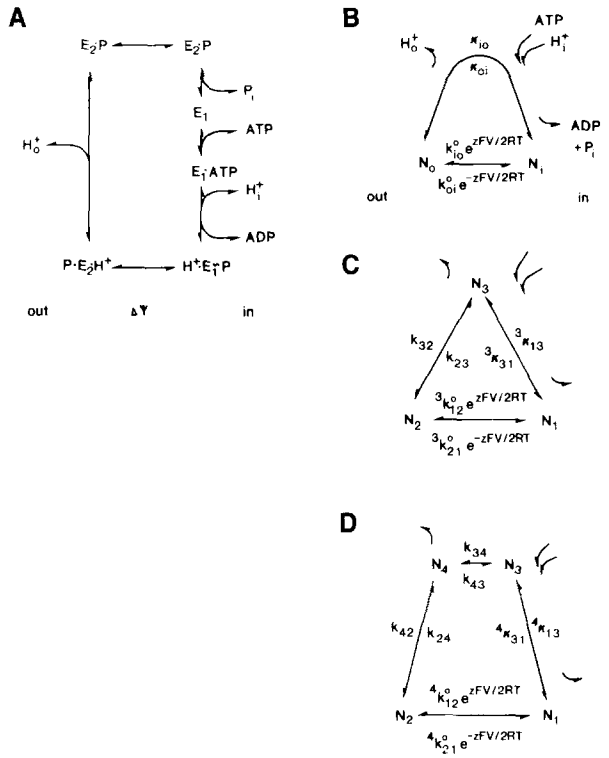

Fig. 1. Carrier cycle for the H^+-ATPase. The carrier cycle (*A*) is modified from the reaction scheme proposed for the Na^+/K^+-ATPase (Karlish et al., 1978) in which, in the forward direction (clockwise), the E_1 form of the enzyme first binds ATP. Proton binding inside hydrolyzes ATP, releasing ADP and energizing the carrier ($H_i^+ \cdot E_1 \sim P$) for conversion to the E_2 form ($H_o^+ \cdot E_2 \cdot P$). The H^+ is released outside, followed by P_i release inside to regenerate the E_1 form again. The cycles in (*B*), (*C*) and (*D*) are equivalent 2-, 3- and 4-state reduction models, respectively, emphasizing the transmembrane charge transfer step ($N_i \rightleftharpoons N_o$, or $N_1 \rightleftharpoons N_2$). Specific assignments for ligand and transportee binding/debinding to reaction constants within the voltage-insensitive limb of the cycles must draw on analyses of changes to the kinetic characteristic evoked by well-defined experimental manipulations

Formally, the pump was described by a simple carrier cycle with a single transport loop and one voltage-dependent transition. Any such model can be 'reduced', for purposes of *I-V* and *dI-V* analysis, to a minimum of two carrier states and four empirical reaction constants (Hansen et al., 1981; Blatt, 1986) as shown in Fig. 1. The carrier states N_i and N_o represented the carrier densities on the inner and outer membrane faces ($N_i + N_o = N$), and membrane charge transit was assigned to a single-state transition characterized by the reaction constants k_{io} and k_{oi}. Voltage sensitivity was introduced (as a first approximation to the unknown voltage profile in the membrane) by means of symmetric Eyring barrier (Läuge & Stark, 1970), so that

$$k_{io} = k_{io}^o e^{zuf2} \text{ and } k_{io} = k_{oi}^o e^{-zuf2} \tag{1a,b}$$

where the specific reaction constants k_{io}^o and k_{oi}^o are voltage independent, their values being defined at zero membrane potential ($V = 0$); z is the net charge transported per carrier cycle (= charge number); the reduced voltage $u = FV/RT$, where F, R, and T have their usual meanings; and the factor 2 places the potential (Eyring) barrier symmetrically within the membrane. The remaining, voltage-independent transitions were lumped into a single step described by the empirical constants κ_{io} and κ_{oi} which, thus, subsumed ATP-, ADP-, inorganic phosphate- and ion- (transportee-) binding and debinding steps, as well as carrier recycling. The full equation for steady-state pump current at any membrane potential was

$$i_P = zFN \frac{k_{io}\kappa_{oi} + k_{oi}\kappa_{io}}{k_{io} + k_{oi} + \kappa_{io} + \kappa_{oi}}. \tag{2}$$

To isolate H^+ binding/debinding steps at the outer membrane surface, the model was expanded (*see* Gradmann, Klieber & Hansen, 1987) by including additional carrier states. For this purpose, a nomenclature analogous to that of Sanders et al. (1984); *see also* Hansen et al., 1981; Slayman & Sanders, 1985; Blatt & Slayman, 1987) was adopted. The minimum model isolating transportee binding/debinding included a third carrier state (Fig. 1), so that

$$i_P = zFN \frac{{}^3k_{12}k_{23}{}^3\kappa_{31} - {}^3k_{21}k_{32}{}^3\kappa_{13}}{{}^3k_{12}(k_{23} + k_{32} + {}^3\kappa_{31}) + {}^3k_{21}({}^3\kappa_{13} + {}^3\kappa_{31} + k_{32}) + {}^3\kappa_{13}(k_{23} + k_{32}) + {}^3\kappa_{31}k_{23}} \tag{3}$$

where ${}^3k_{12}$ and ${}^3k_{21}$ were the 3-state (denoted by superscript), voltage-dependent reaction constants analogous to k_{io} and k_{oi}; k_{32} ($= k_{32}^o[H^+]_o$) and k_{23} were assigned initially as the H^+ binding and debinding reaction constants and ${}^3\kappa_{13}$ and ${}^3\kappa_{31}$ subsumed the remaining lumped reaction steps. In this case, the relationships between the 2- and 3-state reaction constants (*see* Gradmann et al., 1987) are given as

$$k_{io}^o = {}^3k_{12}^o/r_1;\ k_{oi}^o = {}^3k_{21}^o/r_2; \tag{4a,b}$$

$$\kappa_{io} = ({}^3\kappa_{13} + k_{32})/(r_1({}^3\kappa_{31} + k_{32})) \tag{4c}$$

and

$$\kappa_{oi} = (k_{23} + {}^3\kappa_{31})/(r_2({}^3\kappa_{31} + k_{32})), \tag{4d}$$

where the reserve constants

$$r_1 = \frac{{}^3\kappa_{31} + {}^3\kappa_{13} + k_{32}}{{}^3\kappa_{31} + k_{32}} \text{ and } r_2 = \frac{{}^3\kappa_{31} + {}^3\kappa_{13} + k_{23}}{{}^3\kappa_{31} + k_{32}}. \tag{4e,f}$$

Subsequent fittings were carried out also after further expanding the model to include 4 carrier states (Fig. 1), so that

$$i_P = zFN \frac{{}^4k_{12}k_{24}k_{43}{}^4\kappa_{31} - {}^4k_{21}{}^4\kappa_{13}k_{34}k_{42}}{{}^4k_{12}{}^4\kappa_{31}(k_{43} + k_{42}) + k_{42}k_{34}({}^4\kappa_{13} + {}^4k_{12}) + {}^4k_{21}k_{42}(k_{34} + {}^4\kappa_{31}) + {}^4\kappa_{31}k_{43}(k_{24} + {}^4k_{21}) + k_{24}{}^4k_{12}({}^4\kappa_{31} + k_{34}) + {}^4\kappa_{13}{}^4k_{21}(k_{43} + k_{42}) + k_{24}k_{43}({}^4k_{12} + {}^4\kappa_{13}) + {}^4\kappa_{13}k_{34}({}^4k_{21} + k_{24})} \tag{5}$$

where, again, ${}^4k_{12}$ and ${}^4k_{21}$ are the 4-state (denoted by superscript) analogs of k_{io} and k_{oi}. In this case, the H^+ binding and debinding reaction constants were assigned to k_{34} ($= k_{34}^o[H^+]_o$) and k_{43}, respectively. Comparison with the 2-state equivalents (*cf.* Gradmann et al., 1987) yields the relationships

$$k_{io}^{o} = {}^{4}k_{12}^{o} \cdot \frac{{}^{4}\kappa_{31}(k_{43} + k_{42}) + k_{34}k_{42}}{{}^{4}\kappa_{31}(k_{43} + k_{42}) + k_{34}k_{42} + {}^{4}\kappa_{13}(k_{34} + k_{43} + k_{42})} \quad (6a)$$

$$k_{oi}^{o} = {}^{4}k_{21}^{o} \cdot \frac{{}^{4}\kappa_{31}(k_{43} + k_{42}) + k_{34}k_{42}}{{}^{4}\kappa_{31}(k_{43} + k_{42}) + k_{34}k_{42} + k_{24}(k_{43} + k_{34} + {}^{4}\kappa_{31})} \quad (6b)$$

$$\kappa_{io} = \frac{{}^{4}\kappa_{13}k_{34}k_{42}}{{}^{4}\kappa_{31}(k_{43} + k_{42}) + k_{34}k_{42} + {}^{4}\kappa_{13}(k_{43} + k_{42} + k_{34})} \quad (6c)$$

and

$$\kappa_{oi} = \frac{k_{24}k_{43}{}^{4}\kappa_{31}}{{}^{4}\kappa_{31}(k_{43} + k_{42}) + k_{34}k_{42} + k_{24}(k_{43} + {}^{4}\kappa_{31} + k_{34})}. \quad (6d)$$

For least-squares fitting of whole-cell *I-V* data, the nonlinear leak was described empirically by a composite Goldman relation (*see also* Hodgkin & Katz, 1949; Blatt & Slayman, 1987) defined by a "permeability" (P_L, equivalent to a permeability-concentration product for a putative leakage cation) and an equilibrium potential (E_L). The leak current

$$i_L = \frac{F^2}{RT} P_L V \frac{1 - \exp(-F(V - E_L)/RT}{1 - \exp(-FV/RT)}. \quad (7)$$

The full equation for the total membrane current, then, was

$$i_m = i_P + i_L. \quad (8)$$

For the semi-analytical analyses, it was assumed that, at every voltage, changes in whole-cell current were limited to the pump, so that the difference current

$$\Delta i = \Delta i_P = i_P{}^{CN} - i_P^{+CN} \quad (9)$$

where the superscripts denote currents in the absence and presence of CN+SHAM. This approach was restricted to *I-V* (and, hence, *dI-V*) data gathered early on—within the first 3–5 min—during CN exposures. Changes in the leak characteristic were implicated also over this time period from fittings using the other method; but the effect of these changes on currents negative to approximately 0 mV was ignored in the first instance.

Features of the *dI-V* curves [*see* Eqs. (15)–(19) and (26), the Table and accompanying discussion in Blatt; 1986; *see also* Blatt, 1987] were used to find initial parameter weightings based on estimates for the ratios k_{oi}^{o}/k_{io}^{o} and $(\kappa_{io} + \kappa_{oi})/(k_{io}^{o}k_{oi}^{o})^{1/2}$. Fittings of the experimental *dI-V* curves were carried out to Eq. (9) while constraining κ_{oi}, which subsumes ATP and H^+ binding in the forward direction, to a 3 : 1 ratio (−CN : +CN) as an approximation to the observed effect of CN+SHAM on the ATP pool size (*cf.* Roberts et al., 1985; Blatt, 1987). κ_{io}, which subsumes ADP and P_i binding in the reverse direction, was allowed to follow roughly in inverse proportion (*see* Blatt, 1987).

The parent, whole-cell *I-V* curves were reconstructed thereafter according to Eq. (8), the fitted pump parameters and a linear (ohmic) leak current

$$i_L = G_L(V\text{-}E_L) \quad (10)$$

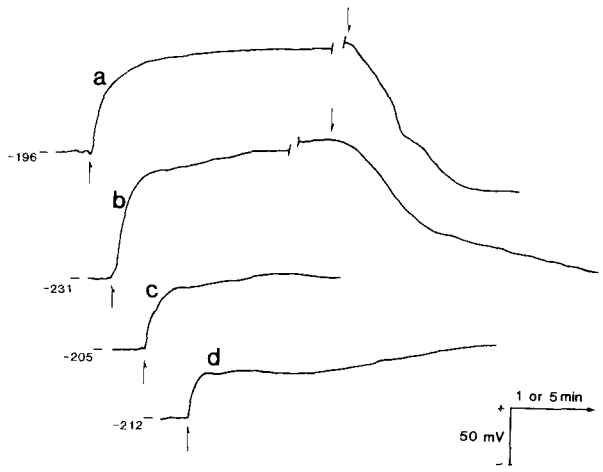

Fig. 2. *Chara* membrane potential response to adding 1 mM NaCN + 0.4 mM SHAM (↑). Voltage traces from three cells (traces *c* and *d* from one cell) showing the time course for depolarization (time scale, 1 min). Recovery on washing out CN+SHAM (traces *a* and *b*, ↓) required 10–20 min (time scale, 5 min). Total time in CN+SHAM: (*a*) 23.5 min, (*b*) 11.2 min

where G_L is the leak conductance. The leak parameters G_L and E_L were determined from the predicted pump currents, which at V_m must just balance current passage through the leak, and from the intersections of the experimental *I-V* curves and the fitted pump characteristic, which define E_L (*see* Blatt, 1987).

Chemicals

Sodium cyanide, SHAM and the pH buffer MES were from Sigma Chemical (St. Louis, MO). Otherwise, all chemicals were analytical grade from BDH (Poole, Dorset, UK).

Where appropriate, results are reported ± SE of (n) observations.

Results

Membrane Potential and ATP Response to CN

Preliminary measurements, recording free-running membrane potentials (V_m) alone, revealed a rapid membrane response to CN+SHAM, but not to SHAM (with 0.1% ethanol) alone. The voltage trajectories from three cells are shown in Fig. 2 and are summarized, along with data from the other cells examined, in Table 1. Free-running (resting) potentials in the absence of CN typically exceeded −200 mV (inside negative) in the standard APW at pH 5.5 (mean, −212 ± 3 mV, n = 13), and thus lay well negative of the equilibrium potentials for any of the dominant diffusion regimes (*cf.* Beilby, 1984).

Adding 1 mM NaCN (+SHAM) resulted in membrane depolarizations (positive-going) with

Table 1. Response of *Chara* leaf cell potentials (V_m) and ATP contents to 1 mM NaCN + 0.4 mM SHAM

		Control	+(CN+SHAM)	$t_{1/2}$/sec
V_m	/mV	−212 ± 3	−119 ± 9	5.4 ± 0.8
[ATP]	/mM	0.74 ± 0.03	0.23 ± 0.02	5.3 ± 0.9

[a] Steady-state membrane potentials were measured before and 120–180 sec after adding CN+SHAM. ATP concentrations and halftimes are from the data in Fig. 3. Halftimes for V_m were pooled from nonlinear least-squares fittings to 13 data sets, including the traces in Fig. 2.

half times of 5.4 ± 0.8 sec (n = 13; range, 4.3–8.7 sec) to potentials between −82 and −158 mV (mean, −119 ± 9 mV, n = 13); over much longer periods in CN+SHAM (10–30 min) V_m frequently decayed further to values positive of −100 mV (−76 ± 6 mV, n = 11). Recovery on washing CN out was slow, but even after prolonged CN treatments (up to 45 min) V_m regained its initial value within 10–20 min of removing the inhibitor (*cf.* Fig. 2, trace *b*).

Parallel measurements of ATP pool size showed in its depletion a similar time course to that for V_m depolarization during metabolic blockade (Table 1). The means of replicate assays (five cells per point) as a function of time in 1 mM CN+SHAM are shown in Fig. 3. Controls without CN (no additions, and 180 sec +SHAM) gave 0.74 ± 0.03 mM ATP (calculated assuming a 7% cytoplasmic volume), in reasonable agreement with Reid and Walker (1983). Adding CN+SHAM resulted in a rapid decay (half time, 5.3 ± 0.9 sec) of ATP content to approximately 32% of the controls. These figures mirror similar measurements from fungal and higher plant tissues (*cf.* Slayman, Long & Lu, 1973; Felle, 1981; Roberts et al., 1985; Blatt, 1987), but contrast with early data (*see* Raven, 1976) gathered without SHAM.

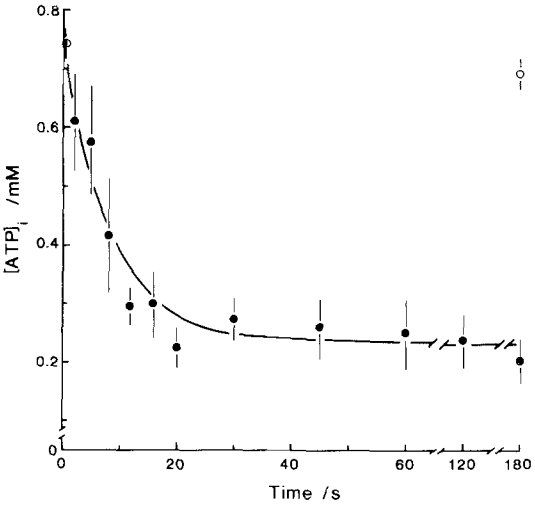

Fig. 3. ATP content of *Chara* leaf cells (◐) and as a function of time after adding 1 mM NaCN + 0.4 mM SHAM (●) or 0.4 mM SHAM alone (○). Each point is the mean ± SE of five cells (except four cells at 2 sec and six cells at 16 sec). Cytoplasmic ATP concentration was determined from the known orthogonal dimensions of each cell assuming a 7% cytoplasmic volume. Data not corrected for assay yields. Data points were fitted by nonlinear least squares (*see* Materials and Methods) to a single falling exponential (solid line). Halftime for decay, 5.3 ± 0.9 sec; final [ATP] predicted, 0.23 ± 0.02 mM

Steady-state *I-V* Response to CN

The full impact of CN at the membrane was revealed on clamping to voltages away from V_m. Figure 4 shows the results of steady-state *I-V* scans from one cell, and the corresponding (slope) conductance-voltage (*G-V*) curves, taken at times before and during exposure to 1 mM NaCN (+0.4 mM SHAM). In the control, the *I-V* curve was distinctly concave to the voltage axis at potentials both positive and negative to V_m before large inward (negative) and outward (positive) currents were recorded at the voltage extremes. Hence, the *G-V* curve showed a prominent maximum near −180 mV.

The predominant effect of CN was to reduce this conductance maximum and the total membrane current near and positive to V_m; for this cell, the short-circuit current (i_{ssc}, at V = 0 mV) dropped by approximately 65% within the first 2 min. Roughly equivalent results were obtained from all of the cells examined. Overall, the effect was to linearize the *I-V* curve over this voltage range, and to drive the free-running potential (*V*-axis intercept) positive-going along the voltage axis. Currents at potentials negative to approximately −300 mV, however, *increased* in magnitude over this same time period. Again, similar results were obtained from all other cells.

dI-V Analysis

It seems reasonable to conclude that the early *I-V* response to CN described above was the direct outcome of ATP withdrawal and a consequent slowing of the pump and membrane depolarization. Nonetheless, steady-state currents, measured as a function of the (clamped) membrane potential, always reflect the sum of all charge-carrying pathways in the membrane. So, the problem is to dissect out those currents specific to pump. Subtracting *I-V* curves ± CN to give a *difference I-V* (*dI-V*) characteristic offers a first approach to isolating the voltage-dependent features for the pump; but the

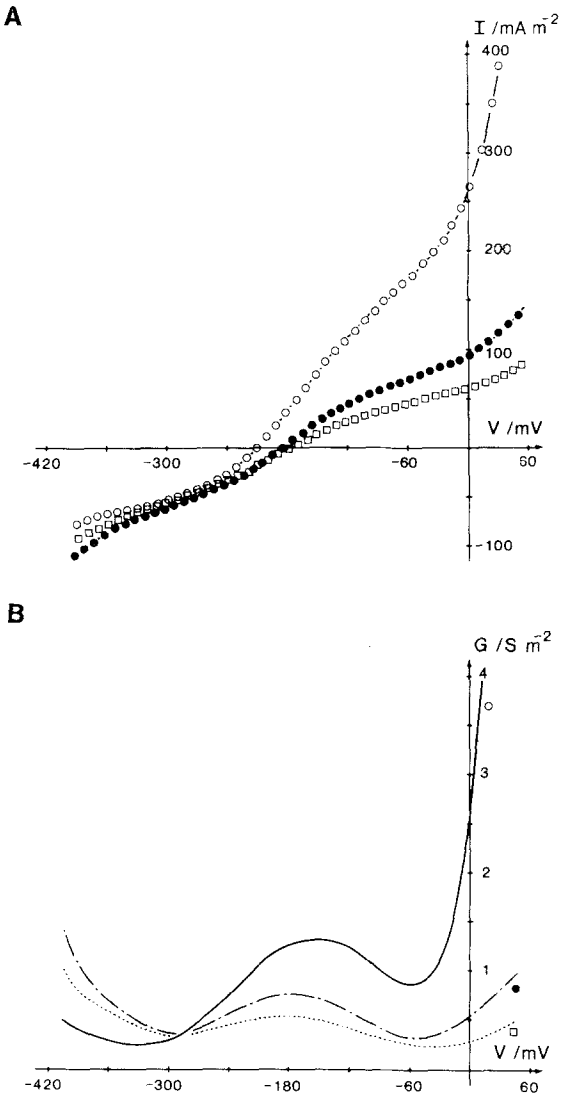

Fig. 4. Steady-state *I-V* response of *Chara* to 1 mM NaCN + 0.4 mM SHAM. (*a*) Current-voltage scans from one cell run immediately before (○), 1.3 (●) and 10 (□) min after adding CN+SHAM. Curves were fitted to 8th order polynomials. (*B*) Slope conductance-voltage (*G-V*) curves derived from differentiating polynomial fittings to the *I-V* curves

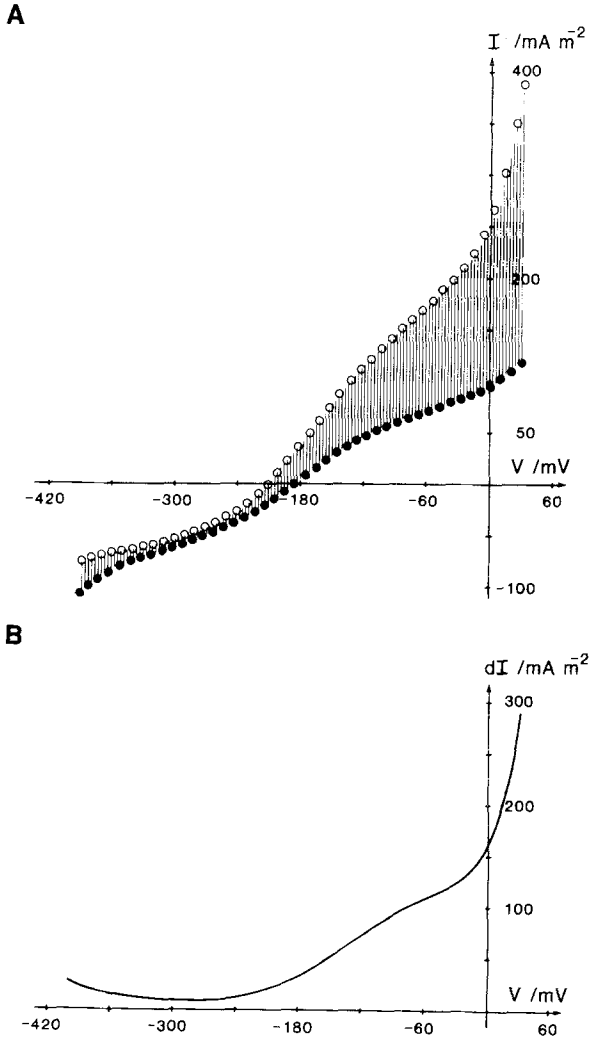

Fig. 5. Difference-current-voltage (*dI-V*, ±CN+SHAM) characteristic for the *Chara* H^+ pump. (*A*) Data of Fig. 4 taken before (○) and 1.3 min (●) after adding 1 mM NaCN + 0.4 mM SHAM. Shading indicates the current difference, and this is replotted in (*B*)

method cannot be expected to yield a reversal (equilibrium) potential for the process directly, simply because the thermodynamic constraints on transport will be affected on withdrawing ATP (Blatt, 1986).

Indeed, as Fig. 5 shows, *dI-V* curves derived from the parent *I-V* data in Fig. 4 wholly failed to cross the voltage axis, even at potentials close to −400 mV. Instead, in approaching the negative voltage extreme currents *increased*, much as has been observed for *dI-V* relations of guard cells in CN (Blatt, 1987) and as Beilby (1984) noted previously in her current subtractions using DES as a pump inhibitor. In the present experiments, comparable results were obtained also in the four other cells analyzed and Fig. 6 illustrates *dI-V* profiles from three of these.

Having recognized the limitations inherent to current subtraction, features of the *dI-V* curves nonetheless can provide important clues to underlying kinetic properties displayed by the pump. If we assume, for the moment, that *all* changes in the whole-cell *I-V* characteristic are attributable to the pump, then subtracting currents ±CN will eliminate the leak from the *dI-V* profile. In this case, two predictions fall directly out of an analytical treatment of carrier kinetics (Blatt, 1986). [We assume that charge transit through the pump is subject to a symmetric potential barrier within the membrane,

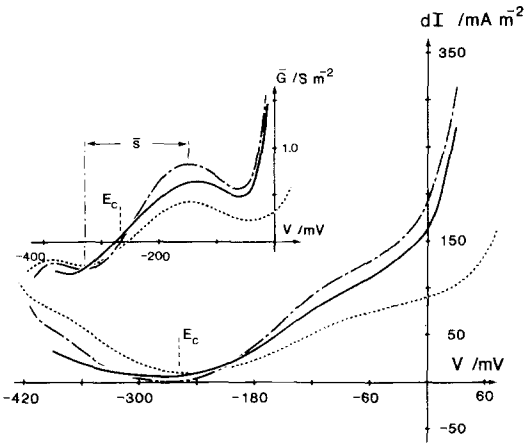

Fig. 6. Difference-current-voltage (*dI-V*) curves from three *Chara* leaf cells. Data obtained by subtracting parent *I-V* curves ±CN+SHAM as illustrated in Fig. 5. Common features in the *dI-V* profile were a minimum about −250 mV and shoulders near −100 and −350 mV. These characteristics give rise in the difference (slope) conductance-voltage ($\bar{G}$-*V*) curves (*inset*) to inflections between −250 and −270 mV (E_c axis of symmetry) and local (±) maxima near −150 and −320 mV [$\bar{s}$, estimated peak-to-peak spread in conductance related to the ratio $(\kappa_{io} + \kappa_{oi})/(k^o_{io}k^o_{oi})^{1/2}$; *see* Blatt, 1986]. For purposes of *dI-V* analysis the large rectifying currents at the voltage extremes were ignored

but it is worth noting that the model is relatively insensitive to deviations from this symmetry (Gadsby & Nakao, 1989).]

First, modifying carrier loading or unloading (e.g., ATP binding) will yield, in the difference current, a *monotonic* (hyperbolic tangent) dependence on voltage only when experimental manipulations affect a *rate-limiting* reaction step. For situations in which this description clearly fails, the peak-to-peak (positive-negative) distance in the difference conductance-voltage ($\bar{G}$-*V*) profile (*see* Fig. 6, inset) can be used to index the relative magnitudes of the two limbs in the reaction cycle [characterized by the ratio $(\kappa_{io} + \kappa_{oi})/(k^o_{io}k^o_{oi})^{1/2}$; *see* Hansen et al., 1981; Blatt, 1986]. Second, *dI-V* profiles will display, independent of the parent *I-V* curves, an axis of symmetry about the equilibrium potential for the voltage-sensitive limb of the cycle

$$E_c = \frac{RT}{zF} \ln(k^o_{oi}/k^o_{io}). \qquad (11)$$

So, a semi-analytic solution to the *dI-V* relation (and, hence, to the parent *I-V* curves) can be sought using information contained within the *dI-V* profile and independent estimates for proportional change(s) incurred in one or more of the reaction constants. Ignoring for the moment the rising currents at the voltage extremes, for the *dI-V* curves in Figs. 5 and 6 an axis of symmetry can be seen about −250 mV, indicating a ratio for k^o_{oi}/k^o_{io} near 10^{-4}. Evident, too, CN can be assumed to have affected a dominant fast reaction, since the *dI-V* profiles were not monotonic; instead, values of 2–10 for the ratio $(\kappa_{io} + \kappa_{oi})/(k^o_{io}k^o_{oi})^{1/2}$ are suggested by the $\bar{G}$-*V* inflections and related peak-to-peak spread, $\bar{s}$ (*see* Fig. 6, inset; *also* Blatt, 1986).

Using these starting estimates, fittings of the experimental *dI-V* curves were carried out to Eq. (9), and the parent whole-cell *I-V* curves were reconstructed thereafter from the fitted pump parameters (Eqs. (8) and (10)). A synopsis of the results for data taken at early times in CN+SHAM are summarized in Table 2; the results for data of Figs. 4 and 5 are shown in Fig. 7. Preliminary fittings were found over a narrow range of parameter values, and for a charge stoichiometry (z) of +1 (but not for integer values of $z > 1$), while constraining κ_{oi} (subsuming ATP binding inside) to the 3:1 ratio (−CN:+CN) dictated by the concentration ratio $[ATP]^{-CN}/[ATP]^{+CN}$. Required, only, was that in CN κ_{io} rose roughly in inverse proportion with κ_{oi}. Since κ_{io} subsumes ADP and P_i binding in the reverse direction, a corresponding rise in these substrates might be inferred (*see* Discussion).

There are operational limits to this interpretation which must be borne in mind. First, absolute values for κ_{io} remained uncertain (*see also* Blatt, 1987); *I-V* scans terminated at the negative extreme short of potentials when pump current could be expected to achieve a voltage independence dictated by values for this reaction constant. Second, near the positive voltage extreme currents and difference currents deviated markedly from the predicted whole-cell *I-V* and pump *dI-V* characteristics. Rectifying currents are expected in the parent *I-V* curves at these voltages; but the fact that a component to these currents appeared in the *dI-V* curve (after subtraction!) can only indicate that they, too, were affected by CN, even within the time frame of 2–5 min.

I-V Analysis

Up to this point, in modeling the electrical response to CN we have maintained that the pump only was affected. Clearly, this assumption cannot hold as treatments are prolonged and secondary effects of metabolic blockade—e.g., cytoplasmic acidification (Sanders & Slayman, 1982) and protein dephosphorylation (*cf.* Stelzer, Kay & Wong, 1988)—come into play. Potassium channel currents in *Chara* (Tester, 1988), as in guard cells (Blatt, 1988*b*), are known to be sensitive to CN, and in

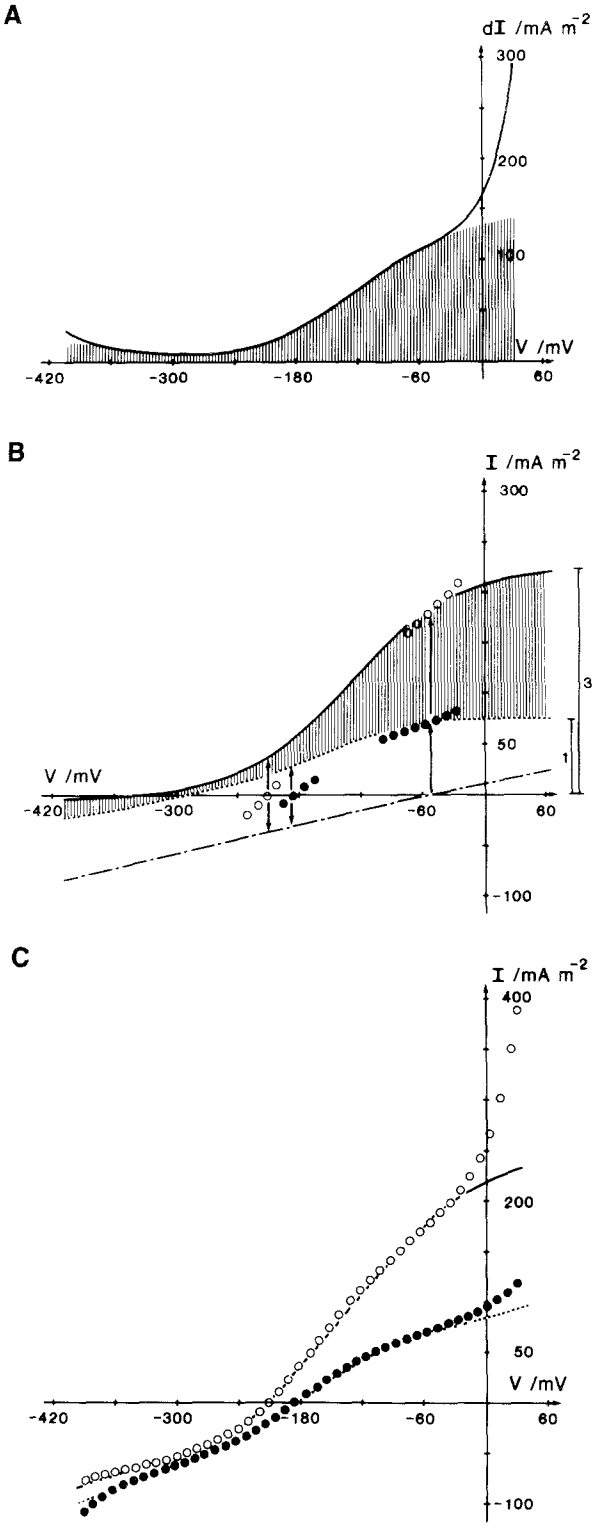

Fig. 7. Fitting the pump-leak model to *Chara* difference-current-voltage (*dI-V*) relations. (*A*) *dI-V* data from Fig. 5 (solid line) and fitted difference currents (shading). (*B*) Modeled pump *I-V* curves yielding the difference currents (shaded) in (*A*). The 3 : 1 (−CN : +CN) constraint on i_{+sat} is indicated on the right. The common leak profile was determined by linear extrapolation from three points. For the first two points, pump currents (↑) at V_m (±CN+SHAM) were mirrored at the voltage axis to obtain the leak currents at these potentials (↓). A third point on the leak (E_L, $i_L = 0$) was defined by the common voltage (−54 mV) at which modeled pump and experimental *I-V* curves intersected. (*C*) Fitted parent *I-V* data. Solid and dotted lines are the modeled pump curves summed with the common linear leak in (*B*). Deviations from the fitted curves near and positive to 0 mV are accommodated by a nonlinear (rectifying leak). Fitted parameters are listed in Table 2

both cases decay progressively over periods of 2–20 min. Also identified in *Chara* is an unspecified leak with a half time for conductance decay in CN on the order of 30–60 sec (*see* Tester, 1988, Fig. 7). Both conductances contribute to rectifying whole-cell currents at positive-going voltages and, in their response to CN would show up quickly as the upward (positive-going) curvature observed at these potentials in the *dI-V* profile as well (*cf.* Fig. 5).

To accommodate these currents within the pump/leak model, we assigned the leak component empirically to a composite Goldman relation (Eq. (7), Materials and Methods); at least from the standpoint of curve fitting, this meant replacing the linear leak parameter G_L with its nonlinear counterpart P_L. However, allowing the leak to vary in CN+SHAM entailed additional degree(s) of freedom which precluded any evaluation restricted to *dI-V* relations alone. Instead, numerical analyses were carried out by least-squares, fitting families of whole-cell *I-V* curves jointly to a sum of model pump and leak currents, while allowing only one or a few of the model parameters (k^o_{io}, k^o_{oi}, κ_{io}, κ_{oi}, P_L and E_L) to vary between curves. Numerical values for each of the parameters, variable and joint, were sought by sequential adjustments using a downhill Simplex method (Nelder & Mead, 1965; Press et al., 1986).

A summary of the model parameters fitted to *I-V* data from the five cells are given in Table 3 and Fig. 8 shows the results with the data of Fig. 4. As was the case in evaluating the corresponding *dI-V* curves, preliminary fittings to the families of *I-V* curves required that κ_{io} and κ_{oi} vary inversely in CN+SHAM. Allowing E_L to vary freely between *I-V* curves did improve fittings for the data of two cells, but the effect was marginal and no consistent trend could be deduced in either case.

However, statistically better and visually satisfactory results (Fig. 8) were obtained only when, in CN+SHAM, P_L declined progressively with time and when the effect on forward operation of the pump cycle was distributed between κ_{oi} and k^o_{io}. Kinetic responses distributed between the two limbs of the reaction cycle are known for situations in which experimental manipulation affects a domi-

Table 2. Kinetic analysis of *Chara* H^+ pump *dI-V* relations and response to 1 mM NaCN + 0.4 mM SHAM at pH_o 5.5[a]

Data set in		Figs. 5 and 7	Summary	
Fitted parameters:				
k^o_{io}	/sec^{-1}	1.6×10^3	1.8×10^3	$\pm 0.3 \times 10^3$
k^o_{oi}	/sec^{-1}	0.12	0.19	± 0.05
κ_{io}	/sec^{-1}	4 (12)	3.7	± 1.1
κ_{oi}	/sec^{-1}	114 (38)	98	±21
Parameter ratios:				
k^o_{oi}/k^o_{io}		7.5×10^{-5}	1.1×10^{-4}	$\pm 0.5 \times 10^{-4}$
$(\kappa_{io} + \kappa_{oi})/(k^o_{io}k^o_{oi})^{1/2}$		6.8	5.7	± 1.3
Derived parameters:				
E_P	/mV	−347	−325	±15
i_{+sat}	/mA m^{-2}	225	190	±37
i_{V_m}	/mA m^{-2}	39	39	± 3
G_{P,V_m}	/S m^{-2}	0.66	0.62	± 0.08
G_L	/S m^{-2}	0.23	0.29	± 0.04
E_L	/mV	−54	−53	± 5

[a] Difference current-voltage data of five cells fitted to Eq. (9) and the minimum 2-state model, and whole-cell *I-V* subsequently reconstructed according to Eqs. (8) and (10), as illustrated in Fig. 7. Parameter and derived values for pump equilibrium potential (E_P), pump current and conductance at saturating positive voltage (i_{+sat}) and at V_m (i_{V_m}, G_{P,V_m}) from the fitting in Fig. 7 are listed separately. Values for κ_{io} and κ_{oi} altered in CN+SHAM are given in parentheses; values summarized are in the absence of CN+SHAM. The pump density (N) is unknown, but it acts as a scalar (Eq. (2)); a value of 2 ± 10^{-8} mol m^{-2} was assumed.

Table 3. Kinetic analysis of *Chara* H^+ pump and leak deduced from *I-V* response to 1 mM NaCN + 0.4 mM SHAM at pH_o 5.5[a]

Data set in NaCN+SHAM		Figs. 4 and 8			Summary	
		○ —	● +1.3 min	□ +10 min		
Fitted parameters:						
k^o_{io}	/sec^{-1}	4.18×10^3	2.57×10^3	2.06×10^3	3.8×10^3	$\pm 0.4 \times 10^3$
k^o_{oi}	/sec^{-1}	0.6	0.6	0.6	0.55	± 0.03
κ_{io}	/sec^{-1}	2.6	29	33	2.4	± 1.3
κ_{oi}	/sec^{-1}	81	36	22	76	±22
Parameter ratios:						
k^o_{oi}/k^o_{io}		1.44×10^{-4}	2.33×10^{-4}	2.92×10^{-4}	1.5×10^{-4}	$\pm 0.3 \times 10^{-4}$
$\frac{(\kappa_{io} + \kappa_{oi})}{(k^o_{io}\kappa^o_{oi})^{1/2}}$		1.7	1.7	1.6	1.7	± 0.4
Derived parameters:						
E_P	/mV	−313	−218	−197	−322	± 7
i_{+sat}	/mA m^{-2}	161	72	43	153	±45
i_{V_m}	/mA m^{-2}	39	15	12	35	± 3
G_{P,V_m}	/S m^{-2}	1.02	0.67	0.54	0.67	± 0.12
G_L	/S m^{-2}	0.21	0.07	0.04	0.22	± 0.04
E_L*	/mV	−82	−82	−82	−64	±10
P_L	/cm^{-2}	1.3×10^{-3}	3.8×10^{-4}	2.0×10^{-4}	6×10^{-4}	$\pm 2 \times 10^{-4}$

[a] Current-voltage data of five cells fitted to Eq. (8) using the minimum 2-state model (Eq. (2)) and nonlinear leak (Eq. (7)). Parameter and derived values for pump equilibrium potential (E_P), pump current and conductance at saturating positive voltage (i_{+sat}) and at V_m (i_{V_m}, G_{P,V_m}) from the fitting in Fig. 8 are listed separately. Values summarized are in the absence of CN+SHAM. The pump density (N) is unknown, but it acts as a scalar (Eq. (2)); a value of 2×10^{-8} mol m^{-2} was assumed.

* Parameter held in common between jointly fitted *I-V* curves.

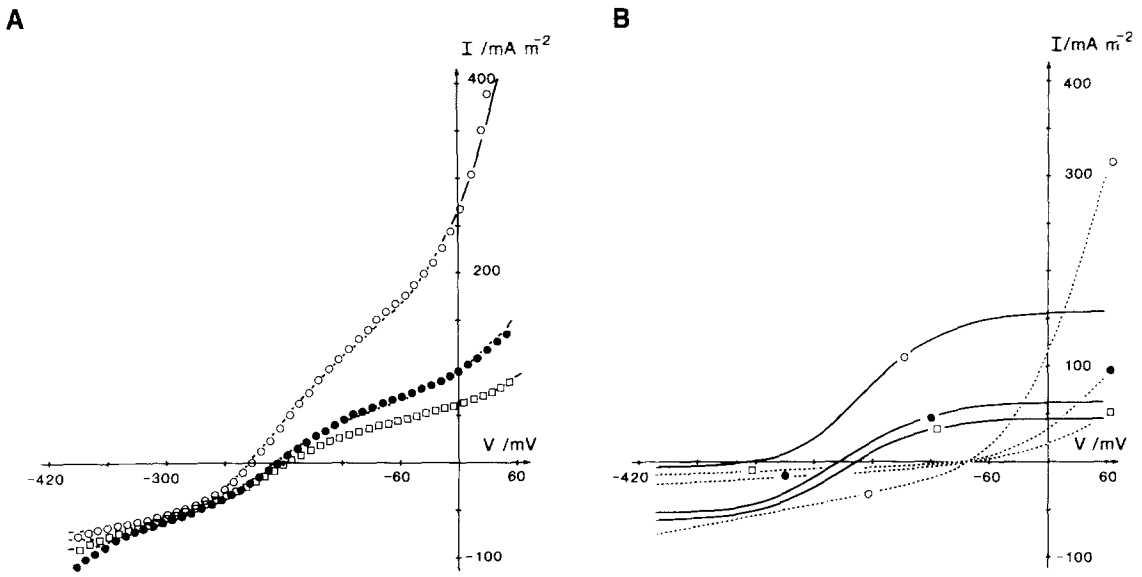

Fig. 8. *Chara* H^+ pump and leak response to 1 mM NaCN + 0.4 mM SHAM. (*A*) Data of Fig. 4 fitted to the sum of pump and nonlinear leak currents. (*B*) Component pump (solid lines) and leak (dotted lines) currents cross-referenced by symbol. Satisfactory fitting to data implicated significant changes to both pump and leak characteristics, even over the first 1.3 min of this experiment. Fitted 2-state pump and leak parameter values are listed in Table 3. Comparable fittings were found for all other data sets

nant fast reaction adjacent to the charge transit step ("transfer effects," *see* Hansen et al., 1981), and we return to this point shortly. Overall, the resultant parameter weightings were roughly equivalent to those predicted from analyses of the *dI-V* relations (*see* Table 2), and the favorable comparison clearly justifies the latter, semi-analytical method. The *I-V* fittings are distinguished in CN+SHAM by markedly larger (negative) pump currents near the negative voltage limit (Fig. 8*B*) which determine the lumped constant κ_{io} (*compare* Tables 2 and 3). Again, values for κ_{io} must be viewed with caution, in this case because the currents arise, in the fitting, from the description of the leak and its response to CN+SHAM (detailed in Discussion).

Kinetic Response to pH_o

As we noted before, there is a strong resemblance between the *dI-V* relations ±CN and those Beilby obtained previously ±DES. However, fundamental differences in the assumptions underlying the kinetic treatments are most outstanding. So, it was of some interest to know whether these earlier data could be brought within the embrace of the concepts and analyses outlined above. The *dI-V* curves ±DES (*cf.* Beilby, 1984, Fig. 15) suggested a qualitatively similar outcome in this case. Nonetheless, there is no precedent for any particular reaction kinetic interpretation of DES action on the pump. Consequently, a more informative test lay in subjecting to statistical minimization Beilby's family of *I-V* curves taken over a range of pH_o values (Beilby, 1984, Fig. 6).

Preliminary fittings were carried out, as before, using the 2-state model for the pump and the nonlinear leak; the results are included in Table 4. Implicated were changes both in κ_{io}, which subsumed H^+ binding at the outer membrane surface, and in the opposing voltage-dependent constant k_{io}^o. Again, the kinetic displacement to k_{io}^o implicated a dominant fast reaction adjacent to the charge transit step. For a putative H^+ pump the effect of substrate (H^+) concentration on one side of the membrane might be isolated reasonably to a single-state transition and reaction constant. So the model was expanded to include a third state, and the additional two (forward, backward) reaction constants, k_{32} and k_{23} (Eq. (3), Materials and Methods), were assigned initially to H^+ binding and debinding, respectively, at the outer face of the membrane. The remaining voltage-independent transitions were subsumed as before, now within the constants ${}^3\kappa_{13}$ and ${}^3\kappa_{31}$.

Attempts at fitting the *I-V* family jointly, while allowing k_{32} only to vary between curves, quickly proved futile. Combinations of reaction constants which satisfied the voltage-dependent spread of the *I-V* data failed at one or the other end of the accessible voltage spectrum where currents were largely pH insensitive (Fig. 9*A*), and vice versa. Instead, good fittings with a single free reaction constant were obtained only with rapid conversions between

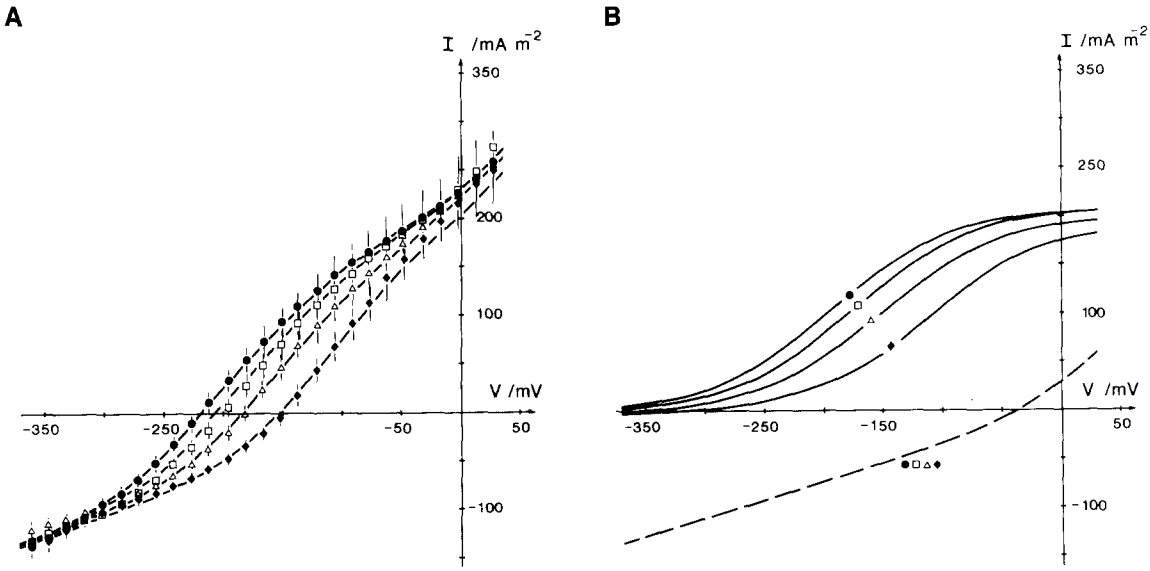

Fig. 9. *Chara* H^+ pump response to extracellular acidification. (*A*) Data of Beilby (1984, Fig. 6; means ± SE from four cells) fitted to the sum of pump and nonlinear leak currents. (*B*) Component pump currents (solid lines) and common leak (dashed line). Fitting indicated acid pH_o shifted the pump *I-V* characteristic right along the voltage axis against a constant leak. Fitted 4-state pump and leak parameter are listed in Table 4

states feeding membrane charge transit on the inside ($^3\kappa_{13}$ and $^3\kappa_{31}$ large) and when $^3\kappa_{13}$ rose, on average, 2.9-fold per $[H^+]_o$ decade. Statistically equivalent fittings were obtained also when both $^3\kappa_{13}$ and k_{32} varied so that their product, $^3\kappa_{13}k_{32}$, rose with $[H^+]_o$ directly, i.e., when E_P was constrained to a (+)58.6 mV shift per $[H^+]_o$ decade where

$$E_P = \frac{RT}{zF} \ln \frac{^3k_{21}^o\,^3\kappa_{13}k_{32}}{^3k_{12}^o k_{23}\,^3\kappa_{31}}. \qquad (12)$$

These parameter values are listed in Table 4.

In principle, the pump cycle might be expanded still further to a maximum of four carrier states and yield an unique solution, provided that this last constraint was restricted to a *single* reaction constant. We sought a 4-state solution under these conditions because, even in the 3-state model, the effect of pH_o could not be isolated sensibly to a single reaction step (in this case, the constant k_{32} adjacent to the membrane charge transit). With a 4-state model, the effect of H_o^+ could be explored at a putative binding step kinetically distant from the $N_2 \rightleftharpoons N_1$ transition.

Fittings were carried out as before, but using Eq. (5) to describe the pump current and tying the reaction constant varying between *I-V* curves to a 1 : 10 : 100 : 1000 (pH_o 7.5 : 6.5 : 5.5 : 4.5) ratio. The effect of pH_o could be approximated over the pH_o range 7.5–5.5, but at pH_o 4.5 dominant features of the fitted curve invariably were right-shifted along the voltage axis relative to the *I-V* data. In fact, the data were gathered originally with only minimal pH_o control (1 mM HEPES and MES buffers) and, at pH_o 4.5, the bathing medium was effectively unbuffered. So we felt justified in relaxing the constraint on the variable constant to a 1 : (7.0–15) : (70–150) : (200–5000) ratio, thereby allowing for an approximate ±0.2 pH unit error margin for the first three curves (pH_o 7.5–5.5) and a ±0.6 pH unit margin for the data at the nominal pH_o 4.5.

In this case, visually and statistically excellent results could be obtained only with k_{34} varying between curves; the final parameter values are included in Table 4, along with the pH_o implied, and the fitted data are shown in Fig. 9. Overall the ordering of constants required for successful fitting with H_o^+ binding subsumed in k_{34} ($= k_{34}^o[H^+]_o$) was

$$^4\kappa_{12}^o,\ ^4\kappa_{13},\ ^4\kappa_{31},\ k_{34}^o \gg k_{43} > k_{24} \gg k_{42},\ ^4k_{21}^o \qquad (13)$$

as summarized in Fig. 10. In effect, this scheme anticipates that the H_o^+-binding/debinding step is kinetically close to the ligand-binding and membrane charge transit steps on the *inside* of the membrane; it predicts a pump which is normally only weakly reversible, even under voltage clamp; and it anticipates that substrate-enhancement (e.g., H_i^+ loading) of the pump will have little effect on output at voltages near and positive to 0 mV. We return to these points in the Discussion.

Table 4. Kinetic analysis of *Chara* H^+ pump response to external pH^a

Pump model and variable parameters		Data set in Fig. 9			
		pH_o 7.5 ●	pH_o 6.5 □	pH_o 5.5 △	pH_o 4.5 ◆
2-State					
k^o_{io}	/sec^{-1}	5.92×10^3	4.08×10^3	1.87×10^3	846
κ_{io}	/sec^{-1}	0.085	0.812	3.22	5.1
3-State					
$^3\kappa_{13}$	/sec^{-1}	136	411	1.03×10^3	3.1×10^3
k_{32}	/sec^{-1}	9.7×10^{-3}	0.032	0.12	0.39
4-State					
k_{34}	/sec^{-1}	40.9	608	4.02×10^3	1.33×10^4
4-State derived parameters:					
E_P	/mV	−457	−388	−340	−309
Equivalent pH_o*		7.50	6.33	5.55	4.99
i_{+sat}	/mA m^{-2}	209	208	200	183
i_{V_m}	/mA m^{-2}	85.4	88.3	70.6	59.1
G_{P,V_m}	/S m^{-2}	0.96	0.96	0.95	0.89
G_{L,V_m}	/S m^{-2}	0.36	0.36	0.37	0.38

[a] Current-voltage data were means ± SE from four cells (Beilby, 1984, Fig. 6) and were fitted to Eq. (8) using the 2- (Eq. (2)), 3- (Eq. (3)) and 4-state (Eq. (5)) models summed with a nonlinear leak (Eq. (7)). Parameter and derived values for pump equilibrium potential (E_P), pump current and conductance at saturating positive voltage (i_{+sat}) and at V_m (i_{V_m}, G_{P,V_m}) are included for the 4-state fitting (*see* Fig. 9). A pump density of 2×10^{-8} mol m^{-2} was assumed for the (unknown) scalar N. Parameters held in common follow. 2-state fitting: k^o_{oi}, 0.11 sec^{-1}; κ_{oi}, 102 sec^{-1}; P_L, 3.85×10^{-4} cm^{-2}; E_L, −35 mV. 3-state fitting: $^3k^o_{12}$, 5.91×10^3 sec^{-1}; $^3k^o_{21}$, 0.061 sec^{-1}; $^3\kappa_{31}$, 4.94×10^3 sec^{-1}; k_{23}, 132 sec^{-1}; P_L, 3.85×10^{-4} cm^{-2}; E_L, −35 mV. 4-state: common parameters: $^4k^o_{12}$, 9.57×10^3 sec^{-1}; $^4k^o_{21}$, 0.10 sec^{-1}; $^4\kappa_{13}$, 7.78×10^3 sec^{-1}; $^4\kappa_{31}$, 8.99×10^3 sec^{-1}; k_{24}, 117 sec^{-1}; k_{42}, 5.60 sec^{-1}; k_{43}, 1.15×10^3 sec^{-1}; P_L, 3.85×10^{-4} cm^{-2}; E_L, −35 mV.

Discussion

Cyanide and the Pump

Over short time periods, metabolic blockade has been shown to be an effective tool for examining primary ion transport as it contributes to the membrane electrical characteristics of *Neurospora* (*cf.* Slayman et al., 1973; Gradmann et al., 1978) and of *Vicia* stomatal guard cells (Blatt, 1987). Paralleling these studies, exposures of *Chara* leaf cells to CN+SHAM depolarized (positive-going) the recorded potentials rapidly and with half times roughly equivalent to those for cytoplasmic ATP depletion; likewise, membrane conductances at the free-running potentials declined, and steady-state *I-V* profiles of the cells linearized within this time frame. Since potentials in the control (−CN) generally lay well negative of all dominant diffusion regimes (*see also* Spanswick, 1974, 1981), these observations are most easily understood in the context of vectorial ion transport coupled directly to ATP hydrolysis. That free-running potentials *in* CN+SHAM generally shifted to values well *positive* of E_K also indicates that membrane conductance to K^+ was low (*see also* Beilby & Blatt, 1986).

Primary Kinetic and Thermodynamic Features of the Pump

By analogy to the effects of CN+SHAM, Beilby (1984) suggested previously that the *Chara* pump could account for conductance decays near V_m in diethylstilbesterol, DES, a known pump antagonist in vitro. Likewise, positive-going displacements in the membrane *I-V* and *G-V* profiles with decreasing pH_o were interpreted in context of the pump being an H^+-ATPase. At a quantitative level, however, the analysis seemed to argue otherwise. Countering the forward operation of a pump, for example by raising the *trans* ion (transportee) concentration, should promote pump operation in the reverse direction; yet, *increasing* $[H^+]_o$ appeared to have no effect on transport rate at (presumed) saturating negative voltages, and the kinetic interpretation paradoxically assigned pump response to a *decrease* in the inherent rate of carrier cycling in the

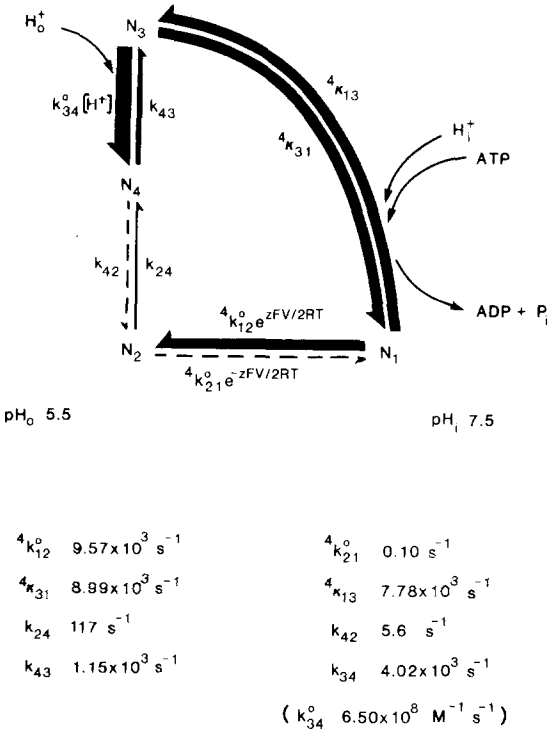

Fig. 10. Reaction kinetic cycle for the *Chara* H^+ pump. Line weights drawn to convey the relative magnitudes for the reaction constants ($^4k_{12}^o$, $^4k_{21}^o$ and k_{34}^o weighted for specific conditions V = 0 mV and $[H^+]_o$ = 1 M). Key features are (*i*) carrier recycling and ligand binding/debinding steps which are in rapid equilibrium (lumped in $^4\kappa_{13}$ and $^4\kappa_{31}$); (*ii*) a prominent free energy transition during membrane charge transit; and (*iii*) a slow step isolating H_o^+ binding from transmembrane charge transfer in the counterclockwise direction. Details in the text

reverse direction, specifically in the voltage-sensitive constant k_{oi}^o.

Ultimately, this problem is rooted in current subtraction. The previous analyses were carried out using *dI-V* curves (±DES), but mistakenly fitting the difference currents to Eq. (2) rather than Eq. (9) or its equivalent. We find, now, that the parent *I-V* response both to extracellular pH and to metabolic blockade can be modeled successfully in contexts of an H^+-ATPase and a common reaction kinetic cycle containing a single membrane charge transit step and carrying a single charge per turnover across a symmetric potential (Eyring) barrier. Predicted from *I-V* data gathered during CN treatments were declines in the empirical constant κ_{oi}, consistent with observed changes in cellular ATP contents. Likewise, fitting *I-V* data gathered over a range of $[H^+]_o$ required corresponding increases in κ_{io} and in higher *n*-state reaction steps which can subsume reasonably H_o^+-binding at the outer membrane surface.

These results point to a charge stoichiometry of 1(H^+):1(ATP) and an equilibrium potential near −420 mV for the pump when pH_o is close to neutrality. The conclusion accords generally with evidence for H^+ pumps in the Characean algae, in fungi and in higher plants (*see* Introduction), and specifically with observations such as free-running potentials which can exceed (−)350 mV (Lucas, 1982). The same characteristics are consistent also with the pump conductance comprising approximately two-thirds of the total membrane conductance near V_m, much as Beilby (1984) deduced before; but the pump *I-V* curve cannot be described by the simple sigmoid (hyperbolic tangent) function of membrane potential, for which $(k_{io}^o k_{oi}^o)^{1/2} \gg (\kappa_{io} + \kappa_{oi})$, as was mistakenly deduced from the *dI-V* curves before (Beilby, 1984; Kishimoto et al., 1984; Takeuchi et al., 1985). In other words, membrane charge transit ($= k_{12}^o \cdot e^{FV/2RT}$) normally must limit the overall rate of forward cycling and thereby confer a voltage dependence on steady-state pump current, despite values predicted for E_P which are generally situated *100–200 mV negative* to V_m (*see* Tables 2 and 3).

Overall, the analyses ally the H^+ pump of *Chara* to primary ion transport at the *Vicia* guard cell membrane (Blatt, 1987), but they contrast sharply with similar kinetic studies of the *Neurospora* H^+ pump (Gradmann et al., 1982; Slayman & Sanders, 1985). For *Neurospora, I-V* response to metabolic blockade appeared restricted to κ_{oi}, plausibly a consequence of energy charge buffering via adenylate kinase (Gradmann et al., 1982; Slayman & Sanders, 1984). However, in *Chara* and in *Vicia* guard cells, for which it has been possible to extend *I-V* scans to voltages well negative of −300 mV, additional changes can be deduced in κ_{io} which may implicate a significant rise in the $[ADP]_i \cdot [P_i]_i$ concentration product (*see* Roberts et al., 1985; *see also* Blatt, 1987).

A still more fundamental kinetic difference is evident in comparing the relative magnitudes of the reaction constants for the voltage-dependent and voltage-independent limbs of the carrier cycle. For *Neurospora, I-V* response to CN can be accommodated with a pump cycle dominated by inherently rapid membrane charge transit (but *see* Blatt & Slayman, 1987), so that $(k_{io}^o k_{oi}^o)^{1/2} \gg (\kappa_{io} + \kappa_{oi})$. The data predict in the pump current and *dI-V* characteristics a monotonic (hyperbolic tangent) dependence on membrane potential over a relatively narrow voltage range (Hansen et al., 1981; Blatt, 1986). For *Chara* and *Vicia,* however, the voltage-dependent transition does not dominate the reaction $[(k_{io}^o k_{oi}^o)^{1/2} \cong (\kappa_{io} + \kappa_{oi})$; *see* Tables 2 and 3] and so limits the rate of carrier cycling over a much

broader voltage range, a conclusion drawn again from *I-V* and *dI-V* response especially at potentials negative to approximately −300 mV (*see* Figs. 5–8).

Cyanide, Pump Reversibility and the Leak

Broad similarities aside, details of the *I-V* analyses for the CN+SHAM and for the pH_o treatments do appear at odds about the reversibility of the pump, and this point deserves some attention. Specifically, the 4-state parameters deduced from the pH_o fittings predict a pump which is only weakly reversible at negative voltages, also in CN+SHAM. Pump currents near the negative voltage extreme, as predicted by the pH_o analyses, are dominated by the rate-limiting constant k_{42} which effectively isolates pump operation in the reverse direction from the effects of $[ATP]_i$, $[ADP]_i$ and $[P_i]_i$ (subsumed in the $N_1 \rightharpoonup N_3$ transition and constants ${}^4\kappa_{13}$ and ${}^4\kappa_{31}$ of the 4-state model; *see* Fig. 10); the maximum current at saturating negative voltages ($= zFN \cdot \kappa_{io}$) would be expected to remain close to (−)10 mA m^{-2}, hence constituting less than 10% of the current magnitude at saturating positive voltages even in the face of metabolic blockade and a 30-fold drop in the ratio of the constants ${}^4\kappa_{31}/{}^4\kappa_{13}$ (from Eq. (6c,d) and Table 4, third column). Clearly, this behavior contrasts sharply with pump currents deduced, at least from statistical fittings of the *I-V* curves actually taken ±CN+SHAM (Fig. 8*B* and Table 3).

In fact, the quantitative differences between these fittings relate to the handling of the leak, rather than to any fundamental inconsistencies in the kinetic model for the pump. We introduced a nonlinear leak to accommodate outward-rectifying currents in the *I-V* profiles near and positive to 0 mV and their decline in CN+SHAM; but the Constant Field description, while a necessary analytical device, is no less empirical than assuming a linear, and constant leak. On consequence of the nonlinear description is that it "ties" leak currents near the negative voltage extreme to changes in conductance which are evident at more positive voltages; so, *treatments which affect the leak are assumed to do so proportionally across the entire voltage spectrum.*

The feature which distinguishes the analyses, then, is the response of the leak to experimental manipulation. The effect of changing external pH could be ascribed entirely to the pump operating in parallel with a *constant* leak, so changes in leak current are not an issue in this case. For the experiments with CN+SHAM, however, decays in leak conductance (Fig. 4*B*, near and positive to 0 mV) were extrapolated proportionately across the voltage spectrum during fitting, and the balance of the current was assigned to the pump. In other words, the predicted pump *I-V* curve assumed at more negative voltages an additional and "cryptic" current, that is one deduced from *changes* in the leak identified near the *positive* voltage limit.

It will be appreciated that differences between *dI-V* and *I-V* analyses of the same data set (Figs. 7 and 8) arise in precisely the same manner. In the latter case, outward-rectifying currents near 0 mV were accommodated by changes in the leak parameter P_L, but with the result that at voltage negative to E_L the pump *I-V* characteristic was assigned an additional current over and above that deduced from fittings in which the leak was held constant. In fact, assuming a *constant* leak during CN+SHAM treatment yielded visually equivalent results over this voltage range (*compare* Figs. 7*C* and 8*A*, ignoring deviations near and positive to 0 mV) and, consistent with the 4-state prediction, little pump current at saturating negative voltages ±CN+SHAM.

Which approximation for the leak is more reliable? Certainly, secondary effects on membrane charge transport are well documented, both under metabolic blockade and in the presence of "ATPase inhibitors" such as vanadate, DCCD and DES (*cf.* Kiefer & Spanswick, 1978, 1979; Beilby, 1984, 1986; Lew & Spanswick, 1984; Tracey & Gresser, 1986; Blatt, 1987, 1988*b*; Blatt, Rodriguez-Navarro & Slayman, 1987). Specifically, for *Chara* cyanide and DES are known to reduce K^+ channel currents which normally activate on (positive-going) depolarization as well as a rectifying, but as yet uncharacterized leak component (Beilby, 1986; Tester,1988). So, the response in secondary charge transport cannot be ignored, definitely over periods of minutes; at the same time, the voltage-dependences—especially of ion channels (Beilby, 1986; Blatt, 1988*b*; Tester, 1988)—offers grounds to suspect that extrapolating changes in leak currents, as in the analyses of Fig. 8 and Table 3, may lead to overestimating pump currents at the distal voltage extreme. This conclusion finds support in the pH_o analysis, but a definitive answer must await more detailed knowledge of secondary transport characteristics over this voltage range.

Transfer Effects and Energy Barriers

One common feature of the kinetic analyses for the CN+SHAM and pH_o data lies in the apparent displacement to membrane charge transit of changes in chemical energy input localized within the voltage-independent limb of the reaction cycle. Fitting *I-V*

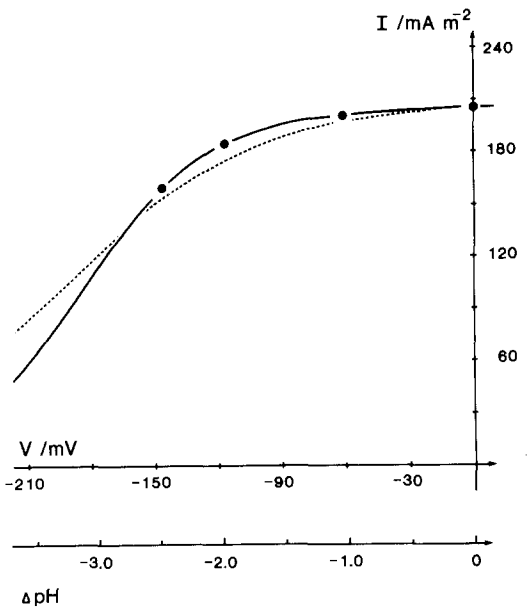

Fig. 11. Equivalence between electrical and chemical driving forces on the *Chara* H^+ pump. Pump current calculated from the 4-state parameters in Table 4. The dotted line is the pump *I-V* curve in the absence of chemical driving force (pH_o 7.5, pH_i = pH_o assumed). The solid curve was calculated at $V = 0$ mV, instead varying k_{34} ($= k^o_{34}[H^+]_o$; $\Delta pH = \log([H^+]_i/[H^+]_o)$). The points are fitted pump short-circuit currents for the data sets in Fig. 9. Electrical and chemical driving forces deviate noticeably beyond approximately −180 mV ($\Delta pH \simeq -3$); over the experimentally accessible pH_o range, however, the difference is never greater than 10% or well within experimental error

response to CN and acid pH_o revealed declines in k^o_{io} which complemented changes in κ_{oi} and/or κ_{io}, subsuming adenylate and inorganic phosphate binding inside and H^+ binding outside. These "transfer effects" (Hansen et al., 1981) can be understood to result on depleting carrier molecules within N_i to adjacent states lumped in the voltage-independent limb of the reaction cycle. It is worth noting, too, that the energetic displacement was restricted to the inner membrane surface, even when experimental manipulations affected transportee (H^+) concentration outside. In other words, the H^+_o-binding step appears kinetically adjacent to charge transit from the *inside* (but not from the outside) of the membrane, with intervening steps necessarily in rapid equilibrium. These characteristics are evident on expansion to a 4-state reaction cycle in which the dominant intermediate states are represented explicitly (Fig. 10). In practical terms, they give rise to an equivalence between changes in chemical and electrical driving force for transport (Fig. 11), a relationship which appears common among H^+-coupled transporters (*cf.* Komor & Tanner, 1980; Blatt et al., 1987) and ATPases (Mitchell, 1969; Hansen et al., 1981; Slayman & Sanders, 1985).

One other feature of the reaction cycle in Fig. 10 stands out. Although ATP hydrolysis (and ADP and P_i release) must take place at a step formally assigned within carrier recycling ($N_3 \rightleftharpoons N_1$ conversion), the major free energy transition occurs in the voltage-sensitive limb of the reaction cycle. From Table 4, the equilibrium potential for charge transit, by analogy with Eq. (11), is −291 mV; for the neutral limb of the cycle, the equilibrium potential (*see* Hansen et al., 1981)

$$E_n = \frac{RT}{F} \ln \frac{^4\kappa_{13} k_{34} k_{42}}{k_{24} k_{43} {}^4\kappa_{31}} \tag{14}$$

at pH_o 5.5 gives −49 mV. Much the same relationship can be deduced from fittings to *I-V* data ±CN in Table 3 (*compare* the ratios k^o_{oi}/k^o_{io} and κ_{io}/κ_{oi}).

This bias in free energy change to the charge transfer reaction accords with Hill and Eisenberg's (1981) proposal that such transitions may be dissociated from energetic input(s) to the cycle; in this case, the transition is synonymous with de-energization of the carrier during transmembrane charge movement. To some extent the interpretation may be consequent on the analytic device of lumping carrier distributions within steps adjacent to the $N_1 \rightharpoonup N_2$ (or $N_i \rightharpoonup N_o$) transition (*see* Gradmann et al., 1987), but it accords with the partial reaction kinetics of at least one other primary ion pump, the Na^+/K^+-ATPase (*cf.* Karlish, Yates & Glynn, 1978; DeWeer, Gadsby & Rakowski, 1988). So far, expansions to a 4-state cycle for the *Neurospora* H^+ pump (Slayman & Sanders, 1985), likewise, support this conclusion. It is worth noting, too, that the estimates for the reaction constants, while on the high side of values expected for a carrier-like transport process, still fall within the range of partial reaction rates deduced from ^{18}O exchange measurements for the H^+-ATPase of *Schizosaccharomyces pombe* (*see* Amoury et al., 1982).

Physiological Implications

The kinetic scheme in Fig. 10 offers an explanation, among others, for the relative insensitivity of pump current to $[H^+]_o$; it also makes a number of quantitative and experimentally testable predictions. Key features are (*i*) carrier recycling and binding/debinding steps at the inner membrane surface that are at rapid equilibrium ($^4\kappa_{13}$ and $^4\kappa_{31}$ large), (*ii*) overall carrier cycling that is rate limited in both directions by a slow step ($N_2 \rightleftharpoons N_4$) isolating membrane charge transit from H^+ binding/debinding

($N_3 \rightharpoonup N_4$) on the outside, and (*iii*) a pK_o of approximately 5.7 ($= \log(k_{43}/k'_{34})$) for H^+_o-binding at the outer membrane surface.

All three points are essential to the pH_o response. Because exit from state N_4 in the reverse direction (k_{42}) is inherently slow, increasing $[H^+]_o$ (k_{34}) will favor carrier accumulating in this state at the expense of the steady-state carrier densities in N_1, N_2 and especially N_3. Thus, the maximum steady-state flux in the forward (clockwise) direction will be reduced, but only when carrier available for ATP and H^+ binding at the inner membrane face becomes depleted, that is when $pH_o \ll pK_o$ *and* $k'_{34}[H^+]_o \gg {}^4\kappa_{31}$. By the same token, current transients following discontinuous voltage steps (both positive- and negative-going) should be reduced under these conditions, since these must draw initially on the carrier densities in states N_1 and N_2 (*see* Bahinski, Nakao & Gadsby, 1988).

Two additional predictions derive immediately from points (*i*) and (*ii*). First, the kinetic description predicts the *Chara* pump normally to be only weakly reversible, both under metabolic restriction (discussed above) and at acid pH_o. Pump turnover in the reverse (counterclockwise) direction is limited by the constant k_{42}, and this effectively dampens the response to raising $[H^+]_o$. Even at extreme negative voltages favoring carrier conversion from state N_2 to N_1 (${}^4k_{21} \ll {}^4k_{12}, k_{24}$), pump current in the reverse direction should approach a fraction only of the maximum forward current obtainable at neutral pH_o, as dictated by the ratio k_{42}/k_{24}.

Second, the model predicts that promoting normal pump operation by substrate enhancement (e.g., by acidifying pH_i) can have little effect on pump current at saturating positive voltages. At these potentials, pump turnover in the forward (clockwise) direction is limited predominantly by k_{24}; the consequences of raising $[H^+]_i$, which must be subsumed within ${}^4\kappa_{31}$, should be masked by this distal rate-limiting step. Instead, the dominant features of the pump *I-V* characteristic are anticipated to shift left (negative-going) along the voltage axis. Projected pump *I-V* curves as a function of pH_i are illustrated in Fig. 12. It is interesting that such a response has been observed for *Vicia* guard cells exposed to fusicoccin, a fungal toxin reputed to lower cytoplasmic pH (Blatt, 1988*a*). Noteworthy, too, the behavior contrasts with pump response in *Neurospora* (Sanders, Hansen & Slayman, 1981; Blatt & Slayman, 1987), for which lowering pH_i approximately 0.8 units augments pump current twofold at saturating positive voltages.

These and related predictions are experimentally approachable, especially in view of the ability to perfuse *Chara* internodes intracellularly. Magnesium ions and ATP are known requirements for generating "electrogenic" membrane potentials in perfused *Chara* (*cf.* Kawamura et al., 1980) and, in a related species *Nitellopsis*, ATP-dependent current

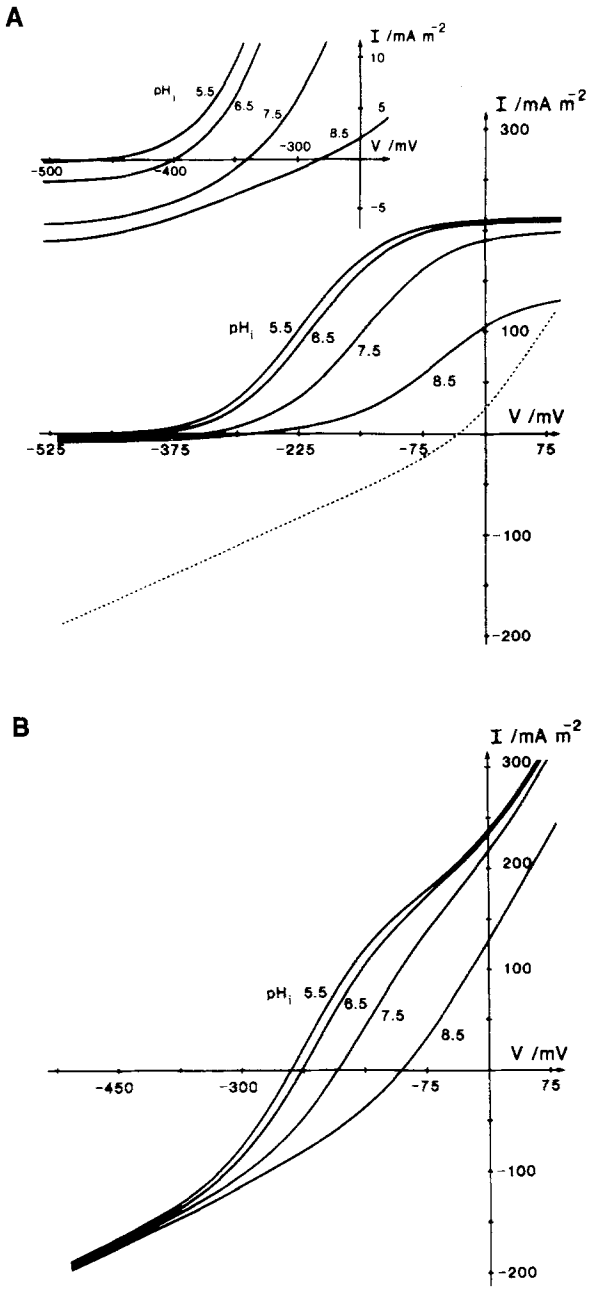

Fig. 12. *Chara* pump response to intracellular pH. (*A*) Predicted pump *I-V* curves (solid lines, pH_i as indicated) calculated from the 4-state parameters in Table 4 and assuming pH_o 5.5. The dotted line is the leak *I-V* profile from Fig. 9. *Inset:* Detail of the predicted pump response close and negative to E_P. (*B*) Predicted whole-cell *I-V* curves constructed by summing the respective pump and leak currents in (*A*). Note that the main effect of acid loading is to shift the dominant features of the curve left along the voltage axis with little change in short-circuit current

correlates with net H^+ extrusion over a range of external and intracellular pH (Takeshige et al., 1986). To date, however, none of these studies have adequately addressed the issue of H^+ pump current *independent* of changes in membrane potential! It remains to be seen now, too, whether $^{32}P_i$ incorporation into ATP can be promoted by priming the pump in the reverse direction, as has been shown with *Acetabularia* (Goldfarb, Sanders & Gradmann, 1984) or, more still, whether ATP hydrolysis is sensitive to acid pH_o and pH_i under voltage clamp at positive potentials.

We are grateful to Dr. D. Kerridge (University of Cambridge, Biochemistry) for putting the luminometer at our disposal. This work was made possible with financial support to M.R.B. and M.J.B. from the Science and Engineering Research Council (UK) and to M.T. from the Royal Commissioners for the Exhibition of 1851.

References

Amoury, A., Goffeau, A., McIntosh, D.B., Boyer, P.D. 1982. Exchange of oxygen between phosphate and water catalyzed by the plasma membrane ATPase from the yeast *Schizosaccharomyces pombe*. *J. Biol. Chem.* **257:**12509–12516

Bahinski, A., Nakao, M., Gadsby, D.C. 1988. Potassium translocation by the Na^+/K^+ pump is voltage insensitive. *Proc. Natl. Acad. Sci. (USA)* **85:**3412–3416

Beilby, M.J. 1984. Current-voltage characteristics of the protein pump at *Chara* plasmalemma: I. pH dependence. *J. Membrane Biol.* **81:**113–126

Beilby, M.J. 1986. Factors controlling the K^+ conductance in *Chara*. *J. Membrane Biol.* **93:**187–193

Beilby, M.J. 1990. Current-voltage curves for plant membrane studies: A critical analysis of the method. *J. Exp. Bot. (in press)*

Beilby, M.J., Beilby, B.N. 1983. Potential dependence of the admittance of *Chara* plasmalemma. *J. Membrane Biol.* **74:**229–245

Beilby, M.J., Blatt, M. 1986. Simultaneous measurements of cytoplasmic K^+ concentration and the plasma membrane electrical parameters in single membrane samples of *Chara*. *Plant Physiol.* **82:**417–422

Bisson, M.A. 1986. Inhibitors of proton pumping: Effect on passive proton transport. *Plant Physiol.* **81:**55–59

Blatt, M.R. 1986. Interpretation of steady-state current-voltage curves: Consequences and implications of current subtraction in transport studies. *J. Membrane Biol.* **92:**91–110

Blatt, M.R. 1987. Electrical characteristics of stomatal guard cells: The contribution of ATP-dependent, "electrogenic" transport revealed by current-voltage and difference-current-voltage analysis. *J. Membrane Biol.* **98:**257–274

Blatt, M.R. 1988*a*. Mechanisms of fusicoccin action: A dominant role for secondary transport in a higher-plant cell. *Planta* **174:**187–200

Blatt, M.R. 1988*b*. Potassium-dependent, bipolar gating of K^+ channels in guard cells. *J. Membrane Biol.* **102:**235–246

Blatt, M.R., Rodriguez-Navarro, A., Slayman, C.L. 1987. Potassium-proton symport in *Neurospora:* Kinetic control by pH and membrane potential. *J. Membrane Biol.* **98:**169–187

Blatt, M.R., Slayman, C.L. 1987. Role of "active" potassium transport in the regulation of cytoplasmic pH by non-animal cells. *Proc. Natl. Acad. Sci. USA* **84:**2737–2741

Chapman, J.B., Johnson, E.A., Kootsey, J.M. 1983. Electrical and biochemical properties of an enzyme model of the sodium pump. *J. Membrane Biol.* **74:**139–153

DeWeer, P., Gadsby, D.C., Rakowski, R.F. 1988. Voltage dependence of the Na-K pump. *Annu. Rev. Physiol.* **50:**225–241

Felle, H. 1981. A study of the current-voltage relationships of electrogenic active and passive membrane elements in *Riccia fluitans*. *Biochim. Biophys. Acta* **646:**151–160

Gadsby, D.C., Nakao, M. 1989. Steady-state current-voltage relationship of the Na/K pump in guinea-pig ventricular myocytes. *J. Gen. Physiol. (in press)*

Goldfarb, V., Sanders, D., Gradmann, D. 1984. Reversal of electrogenic Cl^- pump in *Acetabularia* increases level and ^{32}P labelling of ATP. *J. Exp. Bot.* **35:**645–658

Gradmann, D., Hansen, U.-P., Long, W.S., Slayman, C.L., Warncke, J. 1978. Current-voltage relationships for the plasma membrane and its principal electrogenic pump in *Neurospora crassa:* I Steady-state conditions. *J. Membrane Biol.* **39:**333–367

Gradmann, D., Hansen, U.-P., Slayman, C.L. 1982. Reaction kinetic analysis of current-voltage relationships for electrogenic pumps in *Neurospora* and *Acetabularia*. *Curr. Top. Membr. Transp.* **16:**257–281

Gradmann, D., Klieber, H.-G., Hansen, U.-P. 1987. Reaction kinetic parameters for ion transport from steady-state current-voltage curves. *Biophys. J.* **51:**569–585

Hager, K.M., Mandala, S.M., Davenport, J.W., Speicher, D.W., Benz, E.J., Slayman, C.W. 1986. Amino acid sequence of the plasma membrane ATPase of *Neurospora crassa:* Deduction from genomic and cDNA sequences. *Proc. Natl. Acad. Sci. USA* **83:**7693–7697

Hansen, U.-P., Gradmann, D., Sanders, D., Slayman, C.L. 1981. Interpretation of current-voltage relationships for "active" ion transport systems: I. Steady-state reaction-kinetic analysis of class-I mechanisms. *J. Membrane Biol.* **63:**165–190

Hill, T.L., Eisenberg, E. 1981. Can energy transduction be localized at some crucial part of the enzymatic cycle? *Q. Rev. Biophys.* **14:**463–511

Hodgkin, A.L., Katz, B. 1949. The effect of sodium ions on the electrical activity of the giant axon of the squid. *J. Physiol. (London)* **108:**37–77

Jennings, I., Rea, P., Leigh, R., Sanders, D. 1988. Quantitative and rapid estimation of H^+ fluxes in membrane vesicles. *Plant. Physiol.* **86:**125–133

Karlish, S.J.D., Yates, D.W., Glynn, I.M. 1978. conformational transitions Na^+-bound and K^+-bound forms of the (Na^+ + K^+)-ATPase studied with formycin nucleotides. *Biochim. Biophys. Acta* **525:**252–264

Kawamura, G., Shimmen, T., Tazawa, M. 1980. Dependence of the membrane potential of *Chara* cells on external pH in the presence or absence of internal adenosinetriphosphate. *Planta* **149:**213–218

Keifer, D.W., Spanswick, R.M. 1978. Activity of the electrogenic pump in *Chara corallina* as inferred from measurements of the membrane potential, conductance and potassium permeability. *Plant Physiol.* **62:**653–661

Keifer, D.W., Spanswick, R.M. 1979. Correlation of adenosine triphosphate levels in *Chara corallina* with the activity of the electrogenic pump. *Plant Physiol.* **64:**165–168

Kishimoto, U., Kami-ike, N., Takeuchi, Y., Ohkawa, T. 1984. A kinetic analysis of the electrogenic pump of *Chara corallina:*

I. Inhibition of the pump by DCCD. *J. Membrane Biol.* **80:**175–183

Komor, E., Tanner, W. 1980. Proton-cotransport of sugars in plants. *In:* Plant Membrane Transport: Current Conceptual Issues. R. Spanswick, W. Lucas, and J. Dainty, editors. pp. 247–257. Elsevier, Amsterdam

Läuger, P., Stark, G. 1970. Kinetics of carrier-mediated ion transport across lipid bilayer membranes. *Biochim. Biophys. Acta* **211:**458–466

Lew, R., Spanswick, R.M. 1984. Characterization of the electrogenicity of soybean roots. *Plant. Physiol.* **75:**1–6

Lucas, W.J. 1982. Mechanism of acquisition of exogenous bicarbonate by internodal cells of *Chara corallina*. *Planta* **156:**181–192

Marquardt, D. 1963. An algorithm for least-squares estimation of nonlinear parameters. *J. Soc. Ind. Appl. Math.* **11:**431–441

Mitchell, P. 1969. Chemiosmotic coupling and energy transduction. *Theor. Exp. Biophys.* **2:**159–216

Nelder, J.A., Mead, R. 1965. A simplex method for function minimization. *Comput. J.* **7:**308–313

Press, W., Flannery, B., Teukolsky, S., Vetterling, W. 1986. Numerical Recipies: The Art of Scientific Computing. Cambridge University Press, Cambridge

Raven, J.A. 1976. Transport in algal cells. *In:* Encyclopedia of Plant Physiology, N.S. U. Lüttge and M. Pitman, editors. Vol. 2A, pp. 129–188. Springer Verlag, Berlin—Heidelberg—New York

Reid, R.J., Walker, N.A. 1983. Adenylate concentrations in *Chara:* Variability, effects of inhibitors and relationship to protoplasmic streaming. *Aus. J. Plant Physiol.* **10:**373–383

Richards, J.L., Hope, A.B. 1974. The role of protons in determining membrane electrical characteristics in *Chara corallina*. *J. Membrane Biol.* **16:**121–144

Roberts, J.K.M., Lane, A., Clark, R., Nieman, R. 1985. Relationships between rate of synthesis of ATP and the concentrations of reactants and products of ATP hydrolysis in maize root tips, determined by ^{31}P-NMR. *Arch. Biochem. Biophys.* **240:**712–722

Sanders, D., Hansen, U.-P., Gradmann, D., Slayman, C.L. 1984. Generalized kinetic analysis of ion-driven cotransport systems: A unified interpretation of selective ionic effects on Michaelis parameters. *J. Membrane Biol.* **77:**123–152

Sanders, D., Hansen, U.-P., Slayman, C.L. 1981. Role of the plasma membrane proton pump in pH regulation in non-animal cells. *Proc. Natl. Acad. Sci. USA* **78:**5903–5907

Sanders, D., Slayman, C.L. 1982. Control of intracellular pH: Predominant role of oxidative metabolism, not proton transport, in the eukaryotic microorganism *Neurospora*. *J. Gen. Physiol.* **80:**377–402

Serrano, R., Kielland-Brandt, M.C., Fink, G.R. 1986. Yeast plasma membrane ATPase is essential for growth and has homology with ($Na^+ + K^+$), K^+- and Ca^{2+}-ATPases. *Nature (London)* **319:**689–693

Scott, I.R., Ellar, D.J. 1978. Metabolism and the triggering of germination of *Bacillus megaterium*. *Biochem. J.* **174:**627–634

Shimmen, T., Tazawa, M. 1977. Control of membrane potential and excitability of *Chara* cells with ATP and Mg^{2+}. *J. Membrane Biol.* **37:**167–192

Shimmen, T., Tazawa, M. 1980. Dependence of H^+ efflux on ATP in cells of *Chara australis*. *Plant Cell Physiol.* **21:**1007–1013

Slayman, C.L., Long, W.S., Lu, C.Y.-H. 1973. The relationship between ATP and an electrogenic pump in the plasma membrane of *Neurospora crassa*. *J. Membrane Biol.* **14:**305–338

Slayman, C.L., Sanders, D. 1984. pH-dependence of proton pumping in *Neurospora*. *In:* Hydrogen Ion Transport in Epithelia. pp. 47–56. J.G. Forte, D. G. Warnock, and F. C. Rector, editors. Wiley-Interscience, New York

Slayman, C.L., Sanders, D. 1985. Steady-state kinetic analysis of an electroenzyme. *Symp. Soc. Biochem.* **50:**11–29

Spanswick, R.M. 1972. Evidence for an electrogenic ion pump in *Nitella translucens*. I. The effects of pH, K^+, Na^+, light and temperature on the membrane potential and resistance. *Biochim. Biophys. Acta* **288:**73–89

Spanswick, R.M. 1974. Evidence for an electrogenic ion pump in *Nitella translucens*. II. Control of the light-stimulated component of the membrane potential. *Biochim. Biophys. Acta* **332:**387–398

Spanswick, R.M. 1981. Electrogenic ion pumps. *Annu. Rev. Plant Physiol.* **32:**267–312

Spear, D.J., Barr, J.K., Barr, C.E. 1969. Localization of hydrogen ion and chloride ion fluxes in *Nitella*. *J. Gen. Physiol.* **54:**397–414

Stelzer, A., Kay, A.R., Wong, R.K. S. 1988. $GABA_A$-receptor function in hippocampal cells is maintained by phosphorylation factors. *Science* **241:**339–341

Sze, H. 1985. H^+-translocating ATPases. *Annu. Rev. Plant Physiol.* **36:**175–208

Takeshige, K., Shimmen, T., Tazawa, M. 1986. Quantitative analysis of ATP-dependent H^+ efflux and pump current driven by an electrogenic pump in *Nitellopsis obtusa*. *Plant Cell Physiol.* **27:**337–348

Takeuchi, Y., Kishimoto, U., Ohkawa, T., Kami-ike, N. 1985. A kinetic analysis of the electrogenic pump of *Chara corallina:* II. Dependence of the pump activity on external pH. *J. Membrane Biol.* **86:**17–26

Tester, M. 1988. Pharmacology of K^+ channels in the plasmalemma of the green alga *Chara corallina*. *J. Membrane Biol.* **103:**159–169

Tracey, A., Gresser, M. 1986. Interaction of vanadate with phenol and tyrosine: Implications for the effects of vanadate on systems regulated by tyrosine phosphorylation. *Proc. Natl. Acad. Sci. USA* **83:**609–613

Received 20 June 1989; revised 26 October 1989